STATE SPACE FORMULATION OF TFEA

&

UNCHARTED ISLANDS OF INSTABILITY IN MILLING

A Thesis

presented to

the Faculty of the Graduate School

University of Missouri-Columbia

In Partial Fulfillment

of the Requirements for the Degree

of Masters of Science

---

by

BHAVIN PATEL

Dr. Brian P. Mann, Thesis Supervisor

AUGUST 2007

ACKNOWLEDGMENTS

First a very special thanks to Dr. Brian P. Mann my research adviser for his efforts in guiding my learning process throughout my masters program. Inspite of his busy schedule, he always found adequate time to oversee my studies and helped me progress. Throughout my thesis-writing period, he provided encouragement, sound advice, good teaching, and lots of good ideas. I would have been lost without him. I would also like to thank him for providing me some valuable career advise.

I would also like to thank my committee members Dr. Brian Mann, Dr Roger Fales and Dr. Fan Xudong for their generous commitment.

I wish to thank my family for their continuous support and encouragement.

Needless to say, that I am grateful to all of my colleagues Anupam, Ben, Siddharth and Firas at the Dynamical Systems Laboratory. Finally I wish to thank all my friends at UMC, especially Anagha, Abhijit, Prasad and Abhijit Sarma for their constant moral support.

ABSTRACT

A new approach is developed to examine the stability of delay differential equations that builds upon the previous work in temporal finite element analysis. In contrast to the results of previous work, which could only be applied to second order delay differential equations, the present work is on developing an approach which can be applied to a broader class of systems that may be written in the form of a state space model.

Conclusive evidence that isolated islands of chatter vibration can exist in the stability charts of milling processes is provided. Modeling efforts consider the influence of the tool helix angle to obtain the aforementioned results and develop an analytical force model with three piecewise continuous regions of cutting. Theoretical predictions are validated by a series of experimental tests that confirm the isolated island phenomenon.

Contents

List of Tables

Table **page**

List of Figures

Figure **page**

Chapter 1

INTRODUCTION

1.1 Introduction

Metal removal operations form the major portion of the manufacturing industry‘s ability to make parts with desired shapes, dimensions and surface finish quality. Cost reduction, optimum quality and performance are the main requirements of any manufacturer which can be achieved by designing a predictive model for the metal removing operation. The knowledge of the right cutting parameters serves as tool for optimizing the production. In industries like aerospace and the automobile sector etc, the increasing requirement of high precision, reduced tolerance and high productivity has made it imperative to develop models which can precisely predict the cutting parameters. Milling is one such metal removal operation which has been extensively used in the industry and has complex dynamics.

1.2 Background

Static and dynamic effects during a milling operation cause the system to deviate from the desired geometry. Some of the factors that influence the dynamics of the system are the material properties of the tool and the workpiece, tool geometry, slide speed friction, self-excited and forced oscillations, the cutting parameters such as axial and radial depth of cut and cutting speed. The dynamic effects cause large amplitude vibrations between the cutting tool and the workpiece called chatter and are associated with forced and self-excited oscillations. Chatter is undesirable state as it causes excessive load on the spindle structure, tool wear, inaccurate dimension and poor surface finish. The chatter vibrations are caused as result of both regenerative and non-regenerative effects. Arnold [1] was amongst the first study the regenerative mechanism and showed that the chatter vibration occurred by increasing the cutting speed. Apart from the cutting speed the parameters like the axial and radial depth of cut, spindle speed and feed rate are other factors for chatter vibration. This study did not include the chip thickness variation which was later shown by Tlusty and Polacek [2] and Tobias [3] as important regenerative mechanism that leads to chatter. The graphical representation of the stability information in the form stability charts was first given by Tobias and Fishwick [4] and Tobias [3]. The instability studied in these work was related to loss of stability of a fixed point of an system giving secondary Hopf bifurcation. This work was however limited due to assumption that cutting is a continuous process related to turning process. In turning the orientation of cutting forces and chip thickness are not a function of time, however in milling the cutting forces are explicit function of time. The intermittent nature of milling surfaced as another important cause of chatter vibrations, intermittency introduces a discontinuity into the system. The work of Tlusty and Polacek was one of the first which showed the non-regenerative mechanisms may be a cause of chatter vibrations. Numerical study of non-regenerative mechanisms related due nonlinearities associated

with intermittent nature of milling was done by references [5–8].

1.3 Motivation for the Current Research

With technological advancement in the manufacturing industry and a never ending quest to improve productivity and product quality, high speed milling is incorporated and the process is optimized by high metal removal rates. However the instability in the milling process causes limitation to the application of this technology. Instabilities induce large loads on the spindle structure which might eventually damage the spindle in a long run. The surface finish is also diminished during unstable cutting, which is important where aesthetics, wear resistance etc are concerned. There also is a possibility of deviation in the required geometry of the workpiece, dimensional accuracy is important for components which are used in precision mechanisms, high performance machines etc . The rate of tool wear is another factor that gets affected due to unstable cutting, which may account for considerable increase in the cost of the process. The key solution for this is to better understand dynamics of the system and provide stability charts. Studying the dynamics of milling has shown various phenomenon which causes the undesirable state of cutting. The recent investigation of stability behavior, including the geometry of the tool i.e helix angle of the tool showed some interesting results in the form of isolated islands of instability in the stability plot [9]. Understanding and validating this phenomenon was the primary task for this research.

Analytical stability analysis of the milling process can be found using various methods like semi-discretization, finite element analysis, Temporal finite element analysis (TFEA). The initial efforts to develop TFEA goes to Halley [10] and Bayly *et. al* [11]. This method was improved later by Mann *et. al* [12–14], along with showing

experimental validation of this method. Basically TFEA can deal with delay differential equations which appear in various fields like economics, robotics, population dynamics, biology, and controls using sensors [13,15–17]. However this method is limited to second order DDE's and to increase the scope of application of this method a new approach is build based on the previous work. The state space approach is used for this thesis, and to validate the method it was necessary to look as various DDE's starting with simple autonomous case with scalar control parameters. In addition several of problems that appeared in prior work are analyzed.

1.4 Thesis organization

The new state space approach of TFEA is applied for the DDE's and to check the validity of this approach different class of problems were solved. The Second chapter talks about the new approach showing stability results for scalar autonomous case and generalizing this method for multiple state autonomous case. This is followed by non-autonomous case of continuous time delay in the form of damped delayed Mathieu equation. Further application of this method to a piecewise continuous non-autonomous DDE is also shown. Overall this chapter explains the state space formulation of TFEA. The chapter three deals with milling experimentation. Detailed experiment was done using a flexure which is compliant in one direction, whose governing equation can be mathematically modeled as single degree of freedom equation. The data from the experiments were analyzed and compared with the analytical stability prediction using state space formulation of TFEA. The helix angle of the tool is included in the analysis and the trends for the stability charts are shown comparing different cases of helix angles. The last chapter gives the overall summary of thesis along with possible extension of this work.

Chapter 2

Stability of Delay Equations written as State Space Models

2.1 Introduction

It has been known for quite some time that several systems can be described by models that include past effects. These systems, where the rate of change in a state is determined by both the past and the present states, are described by delay differential equations (DDE). Examples from the recent literature includes applications in robotics, biology, economics and manufacturing processes [13, 15–17]. The qualitative study of a dynamical system often includes a stability analysis, which is presented in form of stability charts that show the stability of the system over a range of system parameters [18–20]. A primary complexity for delay systems lies in the fact that they are of an infinite dimension. In particular, it is well-know that introducing a time delay into a dynamical system causes the phase space to grow from a finite dimension to an infinite dimension [21, 22].

A linear autonomous DDE with a single delay can be described by

$$\dot{\mathbf{y}}(t) = \mathbf{A}\mathbf{y}(t) + \mathbf{B}\mathbf{y}(t-\tau)\,, \tag{2.1}$$

where $\mathbf{A}$ and $\mathbf{B}$ are square matrices and the delay $\tau > 0$. The characteristic equation for the above system, which is obtained assuming that the solution is in exponential form, becomes

$$|\lambda\mathbf{I} - \mathbf{A} - \mathbf{B}e^{-\lambda\tau}| = 0\,. \tag{2.2}$$

As compared to the characteristic equation for an autonomous ordinary differential equation (ODE), Eq. (2.2) has an infinite number of roots. The necessary and sufficient condition for asymptotic stability is that all of the infinite number of characteristic roots must have negative real parts [22]. A discrete solution form for Eq. (2.1) that maps the states of the system over a single delay period, from the $n-1$ period to the n^{th} period, can be written as

$$\mathbf{y}_n = \mathbf{Q}\,\mathbf{y}_{n-1}\,. \tag{2.3}$$

Here, the condition for asymptotically stability requires that the infinite number of characteristic multipliers, or eigenvalues of $\mathbf{Q}$, must be in a modulus of less than one.

Another general case to consider is the stability of a time periodic system with a single delay. The general expression for this type of system is

$$\dot{\mathbf{y}}(t) = \mathbf{A}(t)\mathbf{y}(t) + \mathbf{B}(t)\mathbf{y}(t-\tau)\,, \tag{2.4}$$

where $\mathbf{A}(t+T) = \mathbf{A}(t)$ and $\mathbf{B}(t+T) = \mathbf{B}(t)$. Analogous to time periodic ODE case, the solution can be written in the form $\mathbf{y} = \mathbf{p}(t)e^{\lambda t}$, where $\mathbf{p}(t) = \mathbf{p}(t+T)$. However, a primary difference exist between the dynamic map equation of a time periodic ODE

and a time periodic DDE, which can also be written as Eq. (2.3), since the monodromy operator, $\mathbf{Q}$, for the DDE becomes infinite dimensional. Although the time periodic system will have a finite dimensional Floquet transition matrix, the delay oscillator system will have an infinite dimensional monodromy operator [23]. Also, in contrast to the classical time periodic case, the time delayed system will have an infinite number of characteristic multipliers. The resulting criteria for asymptotic stability requires the infinite number of characteristic multipliers to have a modulus of less than one; this criteria is analogous to requiring the infinite number of characteristic exponents to be negative and real for a continuous system.

The fact that the mondromy operator is infinite dimensional prohibits a closed-formed solution. In spite of this, one can approach this problem from a practical standpoint - by constructing a finite dimensional monodromy operator that closely approximates the stability characteristics of the infinite dimensional monodromy operator. This is the underlying approach that is followed throughout this manuscript and in numerous other previous works use discretization methods to examine delay equations [13, 24, 25]. The results of previous works using the temporal finite element method for delay equations required the governing equations to be written in the form of a second order delay differential equation. A distinguishing feature of the present manuscript is the development of a temporal finite element approach that can be used to determine the stability characteristics of delay differential equations that are in the form of a state space model. Essentially, this work extends the usefulness of the temporal finite element method to a broader class of systems with time delays.

This chapter describes a new approach to examine the stability of delay differential equations that builds upon the work using temporal finite element analysis. In contrast to the results of previous work, which could only be applied to second order delay differential equations, the focus of the present work is on developing an approach which can be applied to a broader class of systems that may be written in

the form of a state space model. A primary result from this work is a generalized formulation to investigate the asymptotic stability of autonomous delay differential equations with a single time delay. Furthermore, this approach is shown to be applicable to time-periodic delay differential equations. Finally, results are also presented to highlight the fact that this methodology can be applied to governing equations that are piecewise continuous.

The content of this chapter is organized as follows. The next section describes the formulation of a temporal finite element analysis approach for autonomous delay equations. In an effort to improve the clarity, the stability of a system with a single state is examined examined prior to presenting a more general analysis that can be applied to autonomous delay differential equations with an arbitrary number of states. The third section examines the subtle differences required to handle systems that are time periodic. Several results are presented for the delayed damped Mathieu Equation prior to examining the case of a milling process. The latter of the two examples highlights a particularly important feature of this method - the ability to handle both continuous and piecewise continuous DDE's.

2.2 Autonomous Delay System

A distinguishing feature of autonomous systems is that time does not explicitly appear in the governing equations. Some application areas where autonomous DDE's arise is in robotics, biology, and control using sensor fusion. In an effort to improve the clarity of this section, we first consider the analysis of a scalar DDE. These results are then followed by an analysis of the general case of a DDE in the matrix vector form.

2.2.1 Scalar Autonomous DDE

Time Finite Element Analysis is an approximate that divides the time intervals of interest into a finite number of temporal elements. This approach allows the original DDE to be transformed into the form of a discrete map. The asymptotic stability of the system is then analyzed from the characteristic multipliers or eigenvalues of the map. While previous works for the TFEA method have solely focused on second order DDE's, the goal here is to present a new approach that is also applicable to first order DDE'S with a single time delay. For instance, consider following time delay system that has a single state variable

$$\dot{y}(t) = \alpha\, y(t) + \beta\, y(t-\tau)\,, \tag{2.5}$$

where α and β are scalar control parameters and τ is the time delay. Since the Eq (2.5) does not have a closed form solution, the first step in the analysis is to consider an approximate solution for the j^{th} element of the n^{th} period as a linear combination of polynomials or trial functions. The assumed solution for the state and the delayed state are

$$y_j(t) = \sum_{i=1}^{3} a_{ji}^{n} \phi_i(\sigma)\ , \tag{2.6a}$$

$$y_j(t-\tau) = \sum_{i=1}^{3} a_{ji}^{n-1} \phi_i(\sigma)\,, \tag{2.6b}$$

where a superscript is used for the coefficients to identify the n^{th} period for the current state and $n-1$ period in the delayed state variable. Each trial function, $\phi_i(\sigma)$, is written as a function of the local time, σ, within the j^{th} element and the local time

is allowed to vary from zero to the time for each element, t_j. The introduction of local time variable is necessary to keep the trial functions orthogonal on the interval $0 \leq \sigma \leq t_j$. To further clarify the local time concept, assume that E elements are used in the analysis and that the time for each element is taken to be uniform, then the time interval for a single element is $t_j = \tau/E$. The polynomials used for this analysis are

$$\phi_1(\sigma_j) = 1 - 23(\frac{\sigma_j}{t_j})^2 + 66(\frac{\sigma_j}{t_j})^3 - 68(\frac{\sigma_j}{t_j})^4 + 24(\frac{\sigma_j}{t_j})^5\,, \tag{2.7a}$$

$$\phi_3(\sigma_j) = 16(\frac{\sigma_j}{t_j})^2 - 32(\frac{\sigma_j}{t_j})^3 + 16(\frac{\sigma_j}{t_j})^4\,, \tag{2.7b}$$

$$\phi_5(\sigma_j) = 7(\frac{\sigma_j}{t_j})^2 - 34(\frac{\sigma_j}{t_j})^3 + 52(\frac{\sigma_j}{t_j})^4 - 24(\frac{\sigma_j}{t_j})^5\,. \tag{2.7c}$$

The above trial functions are orthogonal on the interval of $0 \leq \sigma \leq t_j$ and they are obtained through interpolation. The interpolated trial functions are constructed such that the coefficients of the assumed solution to directly represent the state variables at the beginning $\sigma = 0$, middle $\sigma = t_j/2$, and end $\sigma = t_j$ of each element (see Fig 2.1). The graph in Fig 2.1 illustrates that the coefficients of the assumed solution take on the values of the state variables at specific times. Furthermore, these functions satisfy the natural and essential boundary conditions (i.e. the states at the end of one element match those at the beginning of the following element).

Substituting Eq. (2.6a) and Eq. (2.6b) into Eq. (2.5) results in the following

$$\sum_{i=1}^{3} \left(a_{ji}^n \dot{\phi}_i(\sigma) - \alpha a_{ji}^n \phi_i(\sigma) - \beta a_{ji}^{n-1} \phi_i(\sigma) \right) = \text{error}\,, \tag{2.8}$$

which shows a non-zero error associated with the approximate solutions of Eq. (2.6a) and Eq. (2.6b). In order to minimize this error, the assumed solution is weighted

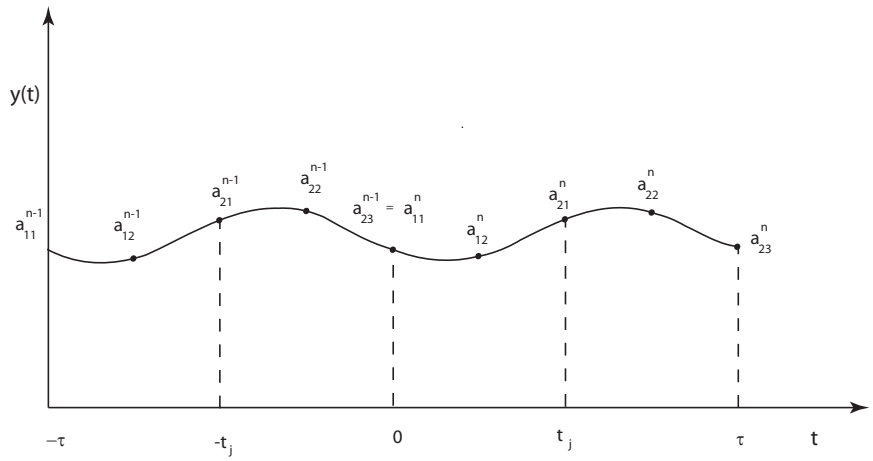

Figure 2.1: Time line of the state variable over an interval of 2π, dots denote location where the coefficients are equivalent to the states and dotted lines mark the beginning and end of each temporal element

by multiplying by a set of test functions, or so called weighting functions, and the integral of the weighted error is set to zero. This is called the method of weighted residuals, are requires that the weighting functions be linearly independent [26]. The weighting functions used for the presented analysis were shifted Legendre polynomials. These polynomials were used because they satisfy the required condition of linear independence. Here, only the first two shifted Legendre polynomials $\psi_1(\sigma) = 1$ and $\psi_2(\sigma) = 2(\sigma/t_j) - 1$ are used. The weighted error expression becomes

$$\int_0^{t_j} \Big(a_{ji}^n \dot{\phi}_i(\sigma) - \alpha a_{ji}^n \phi_i(\sigma) - \beta a_{ji}^{n-1} \phi_i(\sigma) \Big) \psi_p(\sigma) d\sigma = 0\,. \tag{2.9}$$

After applying each weighting function, a global matrix equation can be obtained by combining the resulting equations for each element. To provide a representative expression, we assume two elements are sufficient and write the global matrix of

Eq. (2.10). This equation relates the states of the system in the current period to the states of the system in the previous period.

$$\begin{bmatrix} 1 & 0 & 0 & 0 & 0 \\ N_{11}^1 & N_{12}^1 & N_{13}^1 & 0 & 0 \\ N_{21}^1 & N_{22}^1 & N_{23}^1 & 0 & 0 \\ 0 & 0 & N_{11}^2 & N_{12}^2 & N_{13}^2 \\ 0 & 0 & N_{21}^2 & N_{22}^2 & N_{23}^2 \end{bmatrix} \begin{bmatrix} a_{11} \\ a_{12} \\ a_{21} \\ a_{22} \\ a_{23} \end{bmatrix}^n = \begin{bmatrix} 0 & 0 & 0 & 0 & \Phi \\ P_{11}^1 & P_{12}^1 & P_{13}^1 & 0 & 0 \\ P_{21}^1 & P_{22}^1 & P_{23}^1 & 0 & 0 \\ 0 & 0 & P_{11}^2 & P_{12}^2 & P_{13}^2 \\ 0 & 0 & P_{21}^2 & P_{22}^2 & P_{23}^2 \end{bmatrix} \begin{bmatrix} a_{11} \\ a_{12} \\ a_{21} \\ a_{22} \\ a_{23} \end{bmatrix}^{n-1}, \tag{2.10}$$

The terms inside the matrices of Eq. (2.10) are scalar terms that are given by $\Phi = 1$ and

$$N_{pi}^j = \int_0^{t_j} \Big(\dot{\phi}_i(\sigma) - \alpha\phi_i(\sigma)\Big)\psi_p(\sigma)\, d\sigma\,, \tag{2.11a}$$

$$P_{pi}^j = \int_0^{t_j} \beta\phi_i(\sigma)\psi_p(\sigma)\, d\sigma\,, \tag{2.11b}$$

Eq. (2.10) describes a discrete time system or a dynamic map that can be written in a more compact form $\mathbf{G}\mathbf{a}_n = \mathbf{H}\mathbf{a}_{n-1}$ where the elements of the $\mathbf{G}$ matrix are defined by the each N_{pi}^j term of Eq. (2.11a). Correspondingly, the elements of the $\mathbf{H}$ matrix are defined by the P_{pi}^j terms from Eq. (2.11b). Multiplying the dynamic map expression by $\mathbf{G}^{-1}$ results in $\mathbf{a}_n = \mathbf{Q}\mathbf{a}_{n-1}$ where $\mathbf{Q}= \mathbf{G}^{-1}\mathbf{H}$. Applying the conditions of the chosen trial functions to the beginning, midpoint, and end conditions allows us to replace $\mathbf{a}_n$ and $\mathbf{a}_{n-1}$ with $\mathbf{y}_n$ and $\mathbf{y}_{n-1}$, respectively. Here, $\mathbf{y}_n$ is the vector that represents the state variable at the beginning, middle, end of each temporal finite element. Thus, the the final expression becomes

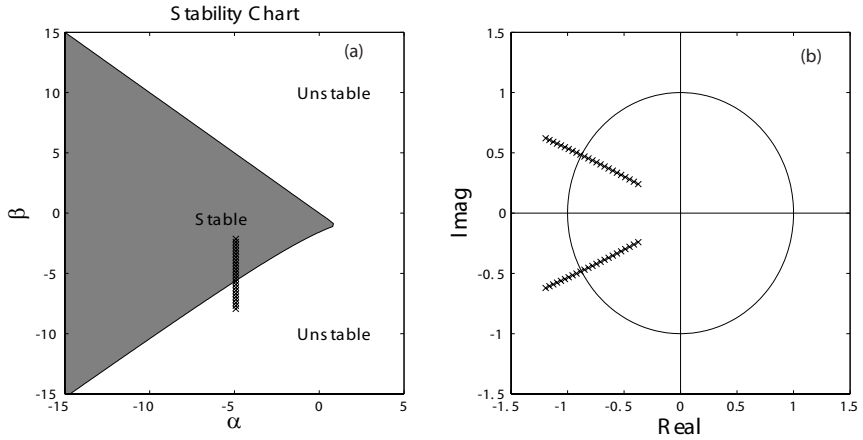

Figure 2.2: Stability Chart for Eq. (2.5) for a single element,, (graph (a)) and CM trajectories in complex plane,(graph (a)).

$$\mathbf{y}_n = \mathbf{Q}\mathbf{y}_{n-1}\,, \tag{2.12}$$

which represents a map of the state variable over a single delay period (i.e the $\mathbf{Q}$ matrix relates the state variable at time instances that correspond to the beginning, middle, and end of each element to the state variable one period into the future).

The eigenvalues of the monodromy operator $\mathbf{Q}$ are called characteristic multipliers (CMs). The criteria for asymptotic stability requires that the magnitudes of the CMs must be in the modulus of less than one for a given combination of the control parameters. The CM trajectories in Figure 2.2(b) shows how the changes in the control parameter causes the CM trajectories pass into the unit circle in a complex plane. The Figure 2.2(a) shows the boundaries between stable and unstable regions as a function of the control parameters α and β. The authors note that the resulting stability chart is identical to the results of Kálmar-Nagy [27]. Before generalizing the

presented approach to autonomous DDE's with an arbitrary number of states, we note that convergence can be obtained by simply increasing the number of elements in the TFEA method [28].

2.2.2 Generalization for Autonomous DDE

While the previous section examined a scalar autonomous DDE, the intent of this section is to generalize the aforementioned approach to the first order DDE's that may have multiple states. The example shown here is often used in modeling the sampling effect in control problems [29]. These systems can be commonly written in the matrix vector form as,

$$\ddot{x}(t) + \alpha\, x(t) = \beta\, x(t-\tau) \tag{2.13}$$

In the above equation, the delay is set to $\tau = 2\pi$ and the terms α and β are used as the system control parameters. The first step in the analysis requires Eq. (2.13) to be written in state space form,

$$\begin{bmatrix} \dot{y}_1 \\ \dot{y}_2 \end{bmatrix} = \begin{bmatrix} 0 & 1 \\ -\alpha & 0 \end{bmatrix} \begin{bmatrix} y_1 \\ y_2 \end{bmatrix} + \begin{bmatrix} 0 & 0 \\ \beta & 0 \end{bmatrix} \begin{bmatrix} y_1(t-\tau) \\ y_2(t-\tau) \end{bmatrix}, \tag{2.14}$$

where $y_1 = x$ and $y_2 = \dot{x}$. At this point, Eq. (2.14) can now be regarded as being identical to Eq. (2.1) which is the general case for an autonomous DDE. The expressions for state and the delayed state variables are now written as vectors

$$\mathbf{y}_j(t) = \sum_{i=1}^{3} \mathbf{a}_{ji}^{n} \phi_i(\sigma) \;, \tag{2.15a}$$

$$\mathbf{y}_j(t-\tau) = \sum_{i=1}^{3} \mathbf{a}_{ji}^{n-1} \phi_i(\sigma) \,. \tag{2.15b}$$

during the j^{th} element. After substituting the assumed solution forms into Eq. (2.14) and using the method of weighted residuals, a global matrix can be obtained that relates the states of the system in the current period to those in the previous period,

$$\begin{bmatrix} \mathbf{I} & 0 & 0 & 0 & 0 \\ \mathbf{N}_{11}^1 & \mathbf{N}_{12}^1 & \mathbf{N}_{13}^1 & 0 & 0 \\ \mathbf{N}_{21}^1 & \mathbf{N}_{22}^1 & \mathbf{N}_{23}^1 & 0 & 0 \\ 0 & 0 & \mathbf{N}_{11}^2 & \mathbf{N}_{12}^2 & \mathbf{N}_{13}^2 \\ 0 & 0 & \mathbf{N}_{21}^2 & \mathbf{N}_{22}^2 & \mathbf{N}_{23}^2 \end{bmatrix} \begin{bmatrix} a_{11} \\ a_{12} \\ a_{21} \\ a_{22} \\ a_{23} \end{bmatrix}^n = \begin{bmatrix} 0 & 0 & 0 & 0 & \mathbf{\Phi} \\ \mathbf{P}_{11}^1 & \mathbf{P}_{12}^1 & \mathbf{P}_{13}^1 & 0 & 0 \\ \mathbf{P}_{21}^1 & \mathbf{P}_{22}^1 & \mathbf{P}_{23}^1 & 0 & 0 \\ 0 & 0 & \mathbf{P}_{11}^2 & \mathbf{P}_{12}^2 & \mathbf{P}_{13}^2 \\ 0 & 0 & \mathbf{P}_{21}^2 & \mathbf{P}_{22}^2 & \mathbf{P}_{23}^2 \end{bmatrix} \begin{bmatrix} a_{11} \\ a_{12} \\ a_{21} \\ a_{22} \\ a_{23} \end{bmatrix}^{n-1} , \tag{2.16}$$

where $\mathbf{I}$ is an identity matrix and the terms $\mathbf{N}_{pi}^j$ and $\mathbf{P}_{pi}^j$ now become the following square matrices

$$\mathbf{N}_{pi}^j = \int_0^{t_j} \Big(\mathbf{I}\dot{\phi}_i(\sigma) - \mathbf{A}\phi_i(\sigma) \Big) \psi_p(\sigma) \, d\sigma \,, \tag{2.17a}$$

$$\mathbf{P}_{pi}^j = \int_0^{t_j} \mathbf{B}\phi_i(\sigma)\psi_p(\sigma) \, d\sigma \,, \tag{2.17b}$$

For this particular system, $\mathbf{\Phi}$ is a 2×2 identity matrix. Using the same criteria for stability as described previously, an example stability chart has been constructed in Fig. 2.3. As noted by references [25,30], the stability chart for this system has stable regions that are in the form of disjoint triangles and stability boundaries with slopes of $\pm$ 1.

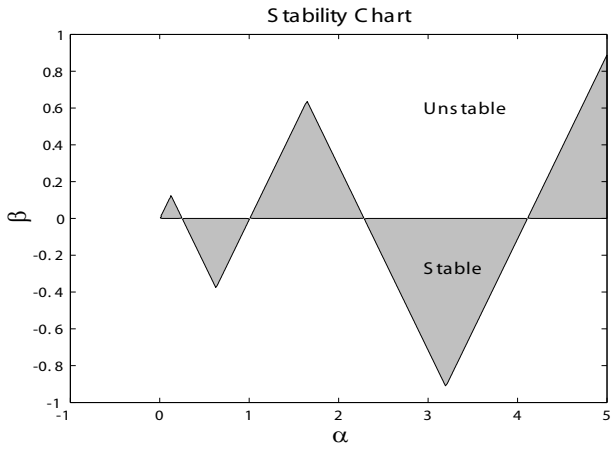

Figure 2.3: Stability chart for the system defined by Eq. (2.13). Stable regions are shaded and unstable regions are left blank.

2.3 Non-autonomous Delay Systems

While both examples from the previous section consider autonomous DDE's, the presented approach can also be applied to non-autonomous DDE's as long as a few subtle changes are implemented. Therefore, the goal of this section is to illustrate the changes required to handle non-autonomous DDE's. Some specific examples where non-autonomous DDE's arise are in controlled systems with base excitation and in manufacturing applications such as milling. More specifically, references [31–33] give the governing equations for a milling process which are shown to contain both a time periodic coefficient and a single time delay.

This sections starts by examining the equations for a continuous non-autonomous system known as the delayed damped Mathieu Equation. This example is followed by the application of the temporal finite element method to a system that is non-autonomous, piecewise continuous, contains a single time delay to highlight the flexibility of the presented approach.

2.3.1 Continuous and Time Periodic DDE

In this section, we consider the Mathieu Equation as the case of a damped and delayed oscillator. The damped delayed Mathieu Equation (DDME) provides as representative system with the combined effect of parametric excitation and a single time delay. The original version of Mathieu's Equation did not contain either damping or a time delay and was discussed first in 1868 by Mathieu [34] to study the vibration of an elliptical membrane. Bellman and Cook [35] and Hsu and Bhatt [36] both made attempts to lay out the criteria for stability using D-subdivision method combined with the theorem of Pontryagin [37]. Insperger and Stépán used analytical and semi-discretization approach in references [23, 38, 39] and Mann *et al.* [40] used a second

order temporal finite element analysis to investigate the stability of the DDME. The equation of interest is

$$\ddot{x}(t) + \kappa\dot{x}(t) + \Big(\delta + \epsilon\cos(\omega\, t)\Big)x(t) = b\, x(t-\tau), \tag{2.18}$$

where the equation has period of $T = 2\pi/\omega$, a damping coefficient of κ, a constant time delay τ=2π. The parameter b acts much like the gain in a state variable feedback system to scales the influence of the delayed term. For the results of this section, the parameter ω is set to one. According to the extended Floquet theory for DDE, this will require the monodromy matrix to be constructed over a period of $T = 2\pi/\omega = 2\pi$.

The first step in the analysis is to rewrite Eq. (2.18) as a state space equation,

$$\begin{bmatrix} \dot{y_1} \\ \dot{y_2} \end{bmatrix} = \begin{bmatrix} 0 & 1 \\ -(\delta + \epsilon\cos(\omega t)) & k \end{bmatrix} \begin{bmatrix} y_1(t) \\ y_2(t) \end{bmatrix} + \begin{bmatrix} 0 & 0 \\ b & 0 \end{bmatrix} \begin{bmatrix} y_1(t-\tau) \\ y_2(t-\tau) \end{bmatrix} \tag{2.19}$$

where $y_1 = x$ and $y_2 = \dot{x}$. Once the equation is written in the form of a state space model, it becomes apparent that the more generalized form is Eq. (2.4). This non-autonomous case has two matrices $\mathbf{A}(t)$ and $\mathbf{B}$ which are given by

$$\mathbf{A}(t) = \begin{bmatrix} 0 & 1 \\ -\delta - \epsilon\cos(\omega t) & k \end{bmatrix}, \qquad \text{and} \qquad \mathbf{B} = \begin{bmatrix} 0 & 0 \\ b & 0 \end{bmatrix}. \tag{2.20}$$

Once again, the solution process starts by substituting Eq. (2.15a) and Eq. (2.15b) into Eq. (2.4). The solution for the j^{th} element then requires a slight alteration to the time periodic terms inside the matrices. Assuming that E uniform temporal

elements are applied, the time duration for each element would be $t_j = T/E$. Next, we substitute $t = \sigma + (j-1)t_j$ into the matrix $A(t)$ so that the cosine term takes on the correct values over the entire period $T = 2\pi/\omega$. These terms are then substituted into Eq. (2.4) and the method of weighted residuals is applied - as in the previous sections. The expressions that populate the matrix of Eq. (2.16) are

$$\mathbf{N}_{pi}^{j} = \int_0^{t_j} \Big(\mathbf{I}\dot{\phi}_i(\sigma) - \mathbf{A}\big(\sigma + (j-1)t_j\big)\,\phi_i(\sigma) \Big) \psi_p(\sigma)\, d\sigma\,, \tag{2.21a}$$

$$\mathbf{P}_{pi}^{j} = \int_0^{t_j} \mathbf{B}\phi_i(\sigma)\psi_p(\sigma)\, d\sigma\,, \tag{2.21b}$$

and $\mathbf{\Phi}$ is taken to be the identity matrix.

The Fig. 2.3.1 shows stability chart for different values of ϵ and κ. It can be seen from stability charts that as the damping is increased the stability properties of the system improves. Also from the three figures in each row it can be observed that the stable parameter space begins to unify as the damping term is increased. At the same time when the amplitude of ϵ is increased due to the effect of parametric excitation the stability regions again start getting disjoint.

2.3.2 Piecewise Continuous and Time Periodic DDE

Delay differential equations are often used to describe the self-excitation of machining processes [24, 41–43]. In order to avoid the regions in the parameter space where self-excited vibrations may exist, one needs to specify the range of parameters (the spindle speed and the depth of cut) at which the process is stable. In this section, we examine the time periodic DDE model for milling that was given by Mann and Young [13]. The equation of interest is

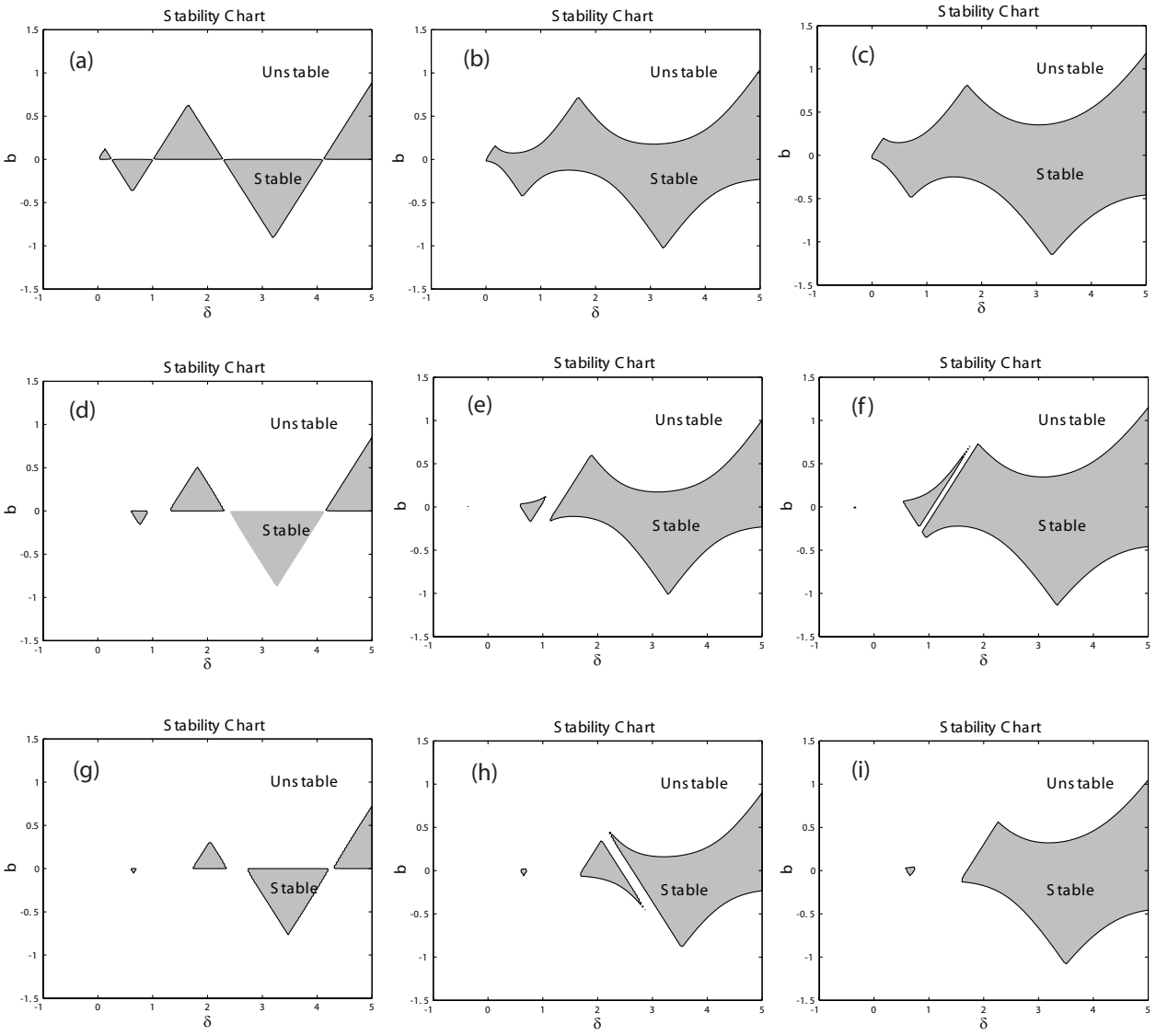

Figure 2.4: Stability chart for Eq. (2.18) using $\tau = 2\pi$. The results of each graph are for the parameters: (a) $\epsilon = 0$ and $\kappa = 0$; (b) $\epsilon = 0$ and $\kappa = 0.1$; (c) $\epsilon = 0$ and $\kappa = 0.2$; (d) $\epsilon = 1$ and $\kappa = 0$: (e) $\epsilon = 1$ and $\kappa = 0.1$; (f) $\epsilon = 1$ and $\kappa = 0.2$; (g) $\epsilon = 2$ and $\kappa = 0$; (h) $\epsilon = 2$ and $\kappa = 0.1$; (i) $\epsilon = 2$ and $\kappa = 0.2$

.

$$\ddot{x}(t) + 2\zeta\omega\dot{x}(t) + \omega^2 x(t) = -b\,K_{sx}(t)\left[x(t) - x(t-\tau)\right], \tag{2.22}$$

where $\zeta = 0.0012$ is the damping ratio, $\omega = 920.5$ is the circular natural frequency, b is the axial depth of cut, and $K_{sx}(t)$ is given by

$$K_{sx}(t) = g_p(t_{en} - t_{ex})[\Gamma_1 \cos\theta_t + \Gamma_2 \sin\theta_t]\sin\theta_t\,, \tag{2.23}$$

where t_{en} is the time when the tool enters the cut and t_{ex} is the time when the tool exits the cut. The Heavyside step function g_p assumes a value of one during the time interval from $t_{en} \leq t \leq t_{ex}$ and is zero for times larger than t_{ex}. This makes milling an example of piecewise continuous system.

Following the same method as shown for damped delayed Mathieu Equation in the earlier part of this section, the first step would be to write the Eq. (2.22) in the state space form which results in

$$\mathbf{A}(t) = \begin{bmatrix} 0 & 1 \\ -\omega^2 - bK_{sx}(t) & -2\zeta\omega \end{bmatrix}, \qquad \text{and} \qquad \mathbf{B}(t) = \begin{bmatrix} 0 & 0 \\ bK_{sx}(t) & 0 \end{bmatrix}. \tag{2.24}$$

As the terms in the matrices $A(t)$ and $B(t)$ are time periodic, we substitute $t = \sigma + (j-1)t_j$ in those matrices so that the periodic terms take the correct values over the entire period. Then the matrices $A(t)$ and $B(t)$ are then substituted in Eq. (2.4) and the method of weighted residuals is applied as in the previous sections.

$$\mathbf{N}_{pi}^{j} = \int_{0}^{t_j} \Big(\mathbf{I}\dot{\phi}_i(\sigma) - \mathbf{A}\big(\sigma + (j-1)t_j\big)\, \phi_i(\sigma) \Big) \psi_p(\sigma)\, d\sigma\,, \tag{2.25a}$$

$$\mathbf{P}_{pi}^{j} = \int_{0}^{t_j} \mathbf{B}\big(\sigma + (j-1)t_j\big)\, \phi_i(\sigma)\psi_p(\sigma)\, d\sigma\,, \tag{2.25b}$$

The expressions Eq. (2.25a) and Eq. (2.25b) are used to populate the matrix Eq. (2.16), where the term $\mathbf{\Phi}$ is defined as a 2×2 matrix Eq. (2.26) and the terms in the matrix are given by Eq. (2.28a) to Eq. (2.28d) in the appendix.

$$\Phi = \begin{bmatrix} \Phi_{11} & \Phi_{12} \\ \Phi_{21} & \Phi_{22}\,, \end{bmatrix} \tag{2.26}$$

Radial Immersion %	θ_{en}	θ_{ex}
5	0	0.1436π
10	0	0.2048π
20	0	0.2952π
50	0	0.5π

Table 2.1: Values of entry and exit angles for up-milling with different percentage of radial immersion

Figure 2.5 and 2.6 show milling stability charts for several different cases of the radial immersion. Here, the radial immersion is defined as the fraction of the tool diameter that engaged in the cut as presented in references [44–46]. However, this can also be expressed solely in terms of entry and exit angles θ_{en} and θ_{ex}, respectively. For instance, the results of Fig. 2.5 are for an up-milling operation which can be defined by the θ_{en} and θ_{ex} values of Table 2.1. The conversion from θ_{en} and θ_{ex} to the values of t_{en} and t_{ex}, terms which give the time interval for g_p to be either one or zero, are given by the following expressions

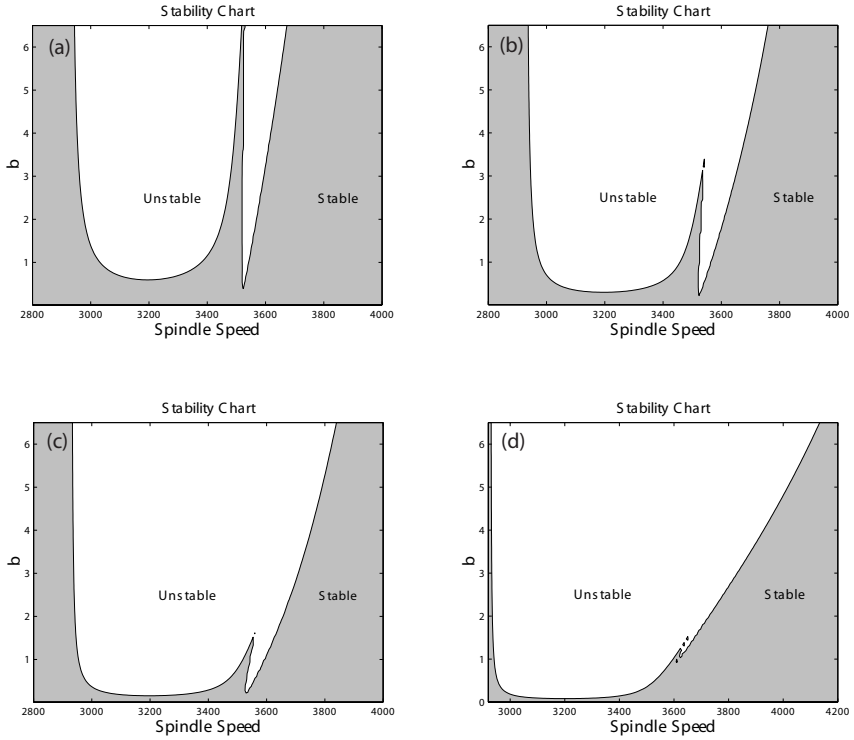

Figure 2.5: Stability Chart for up-milling: with the following percentage radial immersion (a)=5%, (b)=10%, (c)=20% and (d)=50%. The percentage radial immersion corresponds to the θ_{en} and θ_{ex} values given in Table 2.1, the values for t_{en} and t_{ex} are obtained from Eq. (2.27a) and Eq. (2.27b).

$$t_{en} = \frac{\theta_{en}}{\Omega}\,, \tag{2.27a}$$

$$t_{ex} = \frac{\theta_{ex}}{\Omega}\,. \tag{2.27b}$$

where t_{en} and t_{ex} entry and exit times, respectively, θ_{en} and θ_{ex} are the entry and exit angles and Ω is the spindle speed.

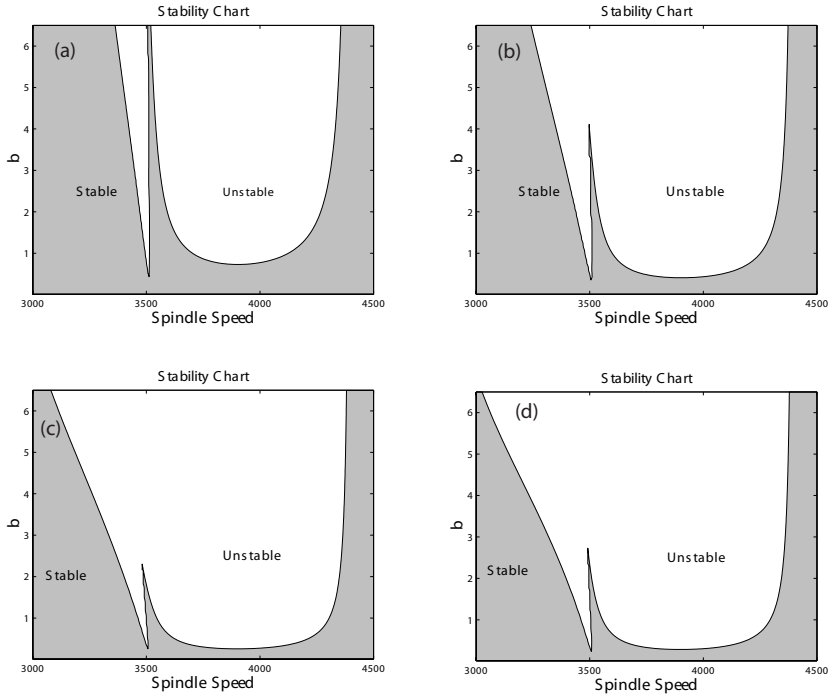

Figure 2.6: Stability Chart for down-milling: with the following percentage radial immersion (a)=5%, (b)=10%, (c)=20% and (d)=50%. The percentage radial immersion corresponds to the θ_{en} and θ_{ex} values given in Table 2.2, the values for t_{en} and t_{ex} are obtained from Eq. (2.27a) and Eq. (2.27b).

The results of Fig. 2.6 corresponds to a down-milling operation with the entry and exit angles listed in the Table 2.2. The corresponding entry and exit times can

Radial Immersion %	θ_{en}	θ_{ex}
5	0.8564π	π
10	0.7952π	π
20	0.7048π	π
50	0.5π	π

Table 2.2: Values of entry and exit angles for down-milling with different percentage of radial immersion

be obtain by the same expressions used for the previous case (i.e. Eq. (2.27a) and Eq. (2.27b), respectively). It can be observed from the Figure 2.5 and 2.6 that the stability charts for up-milling and down-milling are not the same and as the radial immersion is increased the unstable lobes starts merging, reducing the stable region in the stability chart.

2.4 Conclusion

This chapter presents a temporal finite element analysis approach for investigating the stability behavior of linear autonomous and nonautonomous DDE's. In contrast to the results of previous work, which could only be applied to second order DDE's, the present work is applicable to a broader class of systems that may be written in the form of a state space model. The first section describes an introductory example, an autonomous DDE with a single state, prior to generalizing the formulation to autonomous DDE's with multiple states. The examples of the third section extends the presented approach to time-periodic DDE's and highlight the fact that it can be applied to governing equations that are piecewise continuous.

A specific limitation of the presented work is that it is only applicable to DDE's

that contain a single time delay. However, the extension of the presented approach to both nonlinear DDE's and DDE's with multiple time delays is an area of future research.

2.5 Appendix

$$\Phi_{11} = \frac{\lambda_1 e^{\lambda_2 t_f} - \lambda_2 e^{\lambda_1 t_f}}{\lambda_1 - \lambda_2}\,, \tag{2.28a}$$

$$\Phi_{12} = \frac{e^{\lambda_1 t_f} - e^{\lambda_2 t_f}}{\lambda_1 - \lambda_2}\,, \tag{2.28b}$$

$$\Phi_{21} = \frac{\lambda_1 \lambda_2 e^{\lambda_2 t_f} - \lambda_1 \lambda_2 e^{\lambda_1 t_f}}{\lambda_1 - \lambda_2}\,, \tag{2.28c}$$

$$\Phi_{22} = \frac{\lambda_1 e^{\lambda_1 t_f} - \lambda_2 e^{\lambda_2 t_f}}{\lambda_1 - \lambda_2}\,. \tag{2.28d}$$

Chapter 3

Uncharted Islands of Chatter Instability in Milling

3.1 Introduction

The productivity of high speed milling operations is limited by the onset of a self-excited vibration known as chatter [6]. Unless avoided, chatter vibrations may cause large dynamic loads which can damage the machine spindle, cutting tool, or workpiece and leave behind a poor surface finish [6,12,42]. In practice, one of the most prevalent strategies is to simply avoid chatter by applying analyses that predict parameter domains of stable cutting.

While there exist a relatively large body of work that investigates the phenomenon of regenerative chatter [7, 9, 47–49], it is well-known that the pioneering work of Tlusty [2] and Tobias [3, 4] led to the development of stability charts. More specifically, their efforts provided stability charts or lobe diagrams that compactly represented stability information as function of the control parameters in a turning process.

A specific discovery from their work was that the coupling between the cutting forces and tool motion could be captured by including a delay position variable in the governing equations. Thus a number of investigators have targeted this mechanism to predict chatter vibration [5, 15, 50–52]. On the other hand, several authors have also shown that additional physical mechanisms can influence stability such as investigations of nonlinearity [18, 40, 53, 54], thermoplastic behavior in chip formation [55], and frictional effects at the toolchip interface [56].

In comparison to the case of milling, the prior works for turning are only approximate since they rely on the assumption of continuous cutting. In comparison to the case of milling, these prior stability analyses are only approximate since they rely assumption of continuous cutting. In milling, the cutting forces change direction with tool rotation and cutting is interrupted (i.e. zero force values are experienced when the tool is not cutting and a relatively large force is obtained during cutting). The focus of many recent works has been the occurrence of new bifurcation phenomena in interrupted cutting processes. In addition to Neimark-Sacker or secondary Hopf bifurcations, period-doubling bifurcations have now been analytically and/or experimentally shown in several references [20, 49, 57–59].

The phenomena of isolated islands of chatter vibration were first shown to occur in interrupted turning operations by Szalai *et. al* [60]. More recently, Zatarain *et. al* showed a similar phenomenon could occur for helix angle tools in milling processes [9]. Their work used a frequency domain approach to investigate the influence of the helix angle on stability and described some experimental validation. However, the authors used a two-flute end mill for their experiments. Since the experimental validation hinged upon distinguishing the difference between runout and period-doubling, it would have been diffcult to distinguish between these effects without also developing a new approach to recognize chatter under these conditions. In particular, reference [14] shows that runout and period-two motion give nearly indistinguishable frequency

spectra for a two flute tool and other methods are required for chatter detection.

The focus of the current research is to provide independent verifcation of the phenomena described by Zatarain et. al [9]. Furthermore, we believe that conclusive evidence is presented to show isolated islands of chatter vibration do exist in milling processes. The chapter is organized as follows - the first section gives the detailed experimental setup. Followed by the governing equation related to the experimental setup which also includes the derivation for the cutting coefficients for an helical tool. The third section gives an new lytical approach to solve the piece-wise continuous DDE. A separate section on trends in the stability boundaries due to effect of change in helix angle and the radial immersion is presented. This section also shows the changes in stability lobes for different milling operation viz. up-milling and down-milling.

3.2 Description of the Experimental Apparatus

A schematic diagram of the experimental system is shown in the Fig. 3.1. The experimental was designed to mimic a rigid tool and compliant workpiece arrangement which required a flexure that was an order of magnitude more compliant than the cutting tool. Furthermore, the goal was to limit the number of degrees of freedom and focus on the island phenomenon for a relatively simple system. Therefore, the complaint flexure was machined in such that it was only compliant in a single direction. With regards to designing the flexure to have a selected compliance, refer the examples provided within reference [61]

A single non-contact type eddy current displacement transducer was used to measure the displacement and the output of the transducer was filtered using a digital low pass filter and sampled at 25 (KHz), with data acquisition hardware connected to

a laptop computer. A laser tachometer was used to measure a periodic 1/revolution timing pulse using a barcode painted on the spindle as shown in the Fig. 3.1.

Cutting test were performed by feeding the tool along the compliant direction of the flexure which also corresponds to the x-direction of Fig. 3.1. The cutting tool used for the experiments was a three flute, 19.05 (mm) diameter, peripheral end milling with a 30° helix angle. After mounting an aluminum 6061-T6 test specimen onto the flexure, modal parameters were obtained by performing instrumented impact test on both the flexure and cutting tool (see Tab. 3.1). In comparison with the first modal of the flexure, the first modal stiffness of the tool was more than 20 times greater.

The radial immersion is another parameter that is required to describe a given milling process. It can be defined from a combination of two parameters shown in Fig. 3.3. More specifically, the ratio of the radial step over distance, r_s, to the tool diameter, D, is called the radial immersion

$$RI = \frac{r_s}{D} = \frac{1 - \cos\theta_n}{2}\,, \tag{3.1}$$

where θ_n is the angular distance that the tool tip is engaged in cutting. The radial immersion used for all cutting tests was 0.525 or 5.25%.

Table 3.1: Flexure modal parameters and workpiece cutting coefficients.

m (Kg)	ω (rad/s)	ζ	K_n (N/m^2)	K_t (N/m^2)
6.4363	1057.8	0.0056	2.0 $\times 10^8$	5.5 $\times 10^8$

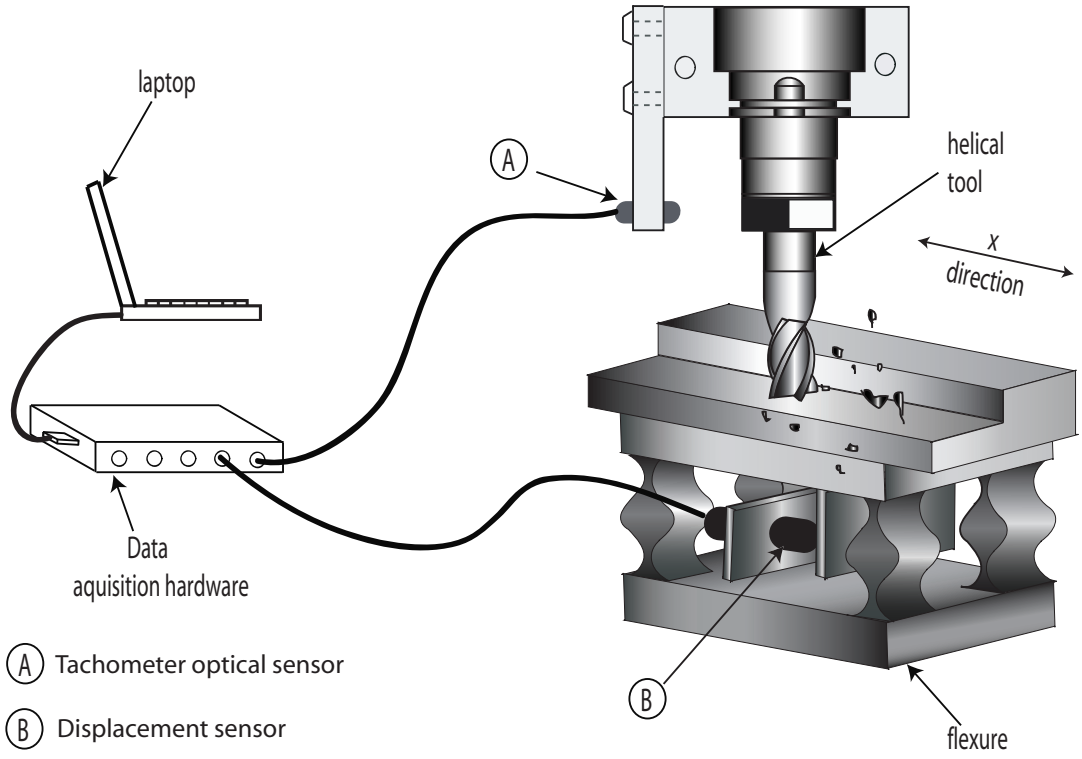

Figure 3.1: Experimental setup for testing stability of single degree of freedom milling

3.3 Milling Process Model

To mimic results of experimental modal tests, the equation of motion is assumed to be the single degree of freedom shown in Fig. 3.3. The mathematical representation of this system is given by

$$\ddot{x} + 2\zeta\omega\dot{x} + \omega^2 x = \frac{1}{m} F_x(t,\tau)\,, \tag{3.2}$$

where ζ is the damping ratio, ω is the circular natural frequency, and m is the modal mass. The final term in the governing equation is the x-direction cutting force, $F_x(t,\tau)$, which is a function of both time and the time delay between consecutive passages of the cutting teeth, τ. The remainder of this section describes the cutting force that is later applied when analyzing the governing equation of motion.

3.3.1 Cutting Force Model

This section derives analytical expressions for the x-direction cutting forces of a helical end mill. A typical peripheral end mill with helical flutes is shown in Fig. 3.2. The tangential and normal forces acting on a differential element of height dz can be expressed as

$$dF_t = g(z,t) K_t w\left(\theta(z,t),\tau\right) dz\ , \tag{3.3a}$$

$$dF_n = g(z,t) K_n w\left(\theta(z,t),\tau\right) dz\ , \tag{3.3b}$$

where $\theta(z,t)$ is the rotation angle of the reference tooth shown in Fig. (3.3a–b). Here, the term 'reference tooth' is applied draw attention to the fact that we have

only written the cutting forces on a single cutting tooth and not for multiple cutting teeth. However, when multiple teeth are engaged in cutting, the total force is found from a summation of the individual forces from each cutting tooth. The expression for the angular orientation of the reference tooth is $\theta(z,t) = \Omega t - \kappa z$ where Ω is the tool rotational speed in (rad/s) and $\kappa = (2\tan\beta)/D$ is defined in terms of the helix angle, β. The function $g(z,t)$ is a Heaviside step function that accounts for the fact that milling is an interrupted cutting process and assumes a value one when the cutting tooth is engaged in cutting and zero when the tool is out of the cut. The cutting coefficients along the tangential and normal directions of the tool are given by K_t and K_n. Following the work of reference [62, 63], a circular tool path is assumed which allows the radial chip thickness for the reference tooth to be written as

$$w\big(\theta(z,t),\tau\big) = h\sin\theta(z,t) + \big[x(t) - x(t-\tau)\big]\sin\theta(z,t)\,, \tag{3.4}$$

where h is the feed per tooth and τ is the time delay between consecutive tooth passages. The cutting force along the compliant direction of the workpiece is obtained by integrating Eq. (3.3a) and Eq. (3.3b) with respect to the differential axial depth, dz. The expression for the reference flute of the tool becomes

$$F_x(t,\tau) = \int_{z_1(t)}^{z_2(t)} -g(z,t)\Big[dF_t\cos\theta(z,t) + dF_n\sin\theta(z,t)\Big]dz\,, \tag{3.5}$$

where the limits of integration $z_1(t)$ and $z_2(t)$ depend upon several conditions. In particular, the limits of integration are piecewise continuous in an entry, middle of the cut, and exit region. The piecewise continuous integration limits mean that analytical cutting force expression of Eq. (3.5) is piecewise continuous in each of the three regions labeled 1–3 of Fig. 3.2. Table 3.3.1 gives the $z_1(t)$ and $z_2(t)$ expressions

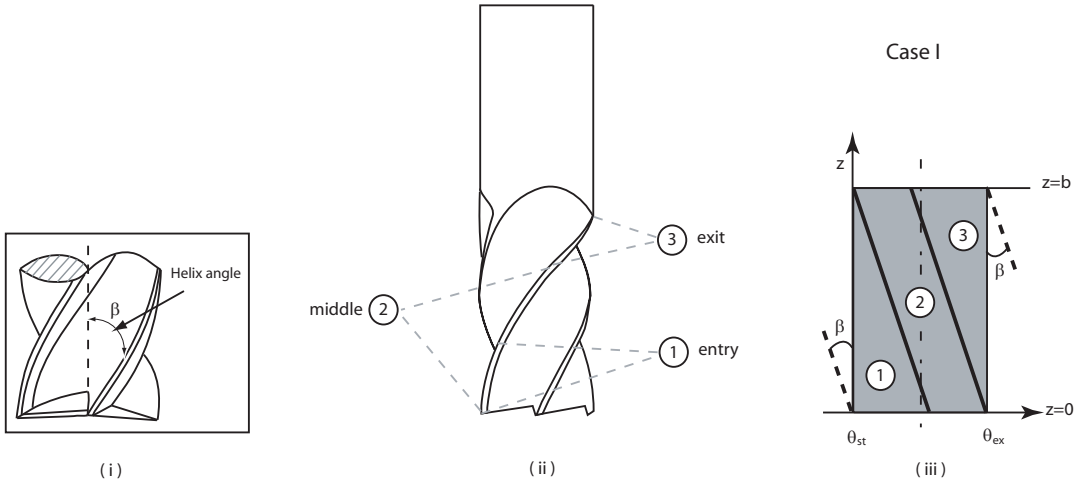

Figure 3.2: Two different cases of helix angle. Each case shows the three regions of consideration 1. entry, 2. middle. and 3. exit with the corresponding values of z

for each cutting regions and for two different cases that might arise. Here, the entry angle depends upon whether up-milling ($\theta_{st} = 0$) or down-milling ($\theta_{st} = \pi - \theta_n$) process is being examined.

To delineate between the two different cases of Table 3.3.1, we first define a new parameter $\kappa = (2\tan\beta)/D$. Here, we conclude that the second case will only arise if the tool tip exits before $z_2(t)$ takes on a value equal to b. For this second case, the upper limit of integration at the instant the tool tip exits, t_{ex}, is given by $z_2(t_{ex}) = \theta_n/\kappa$. Therefore, the second case is applied when $z_2(t_{ex}) < b$ and the first case is applied otherwise.

3.4 Stability Analysis

The goal of this section is to describe a new solution approach for determining the asymptotic stability boundaries for the governing delay differential equation. While

Table 3.2: Integration limits for each situation and cutting region.

Region	Case I	Case II
Entry	$z_1 = 0$ $z_2(t) = (\Omega t - \theta_{st})/\kappa$	$z_1 = 0$ $z_2(t) = (\Omega t - \theta_{st})/\kappa$
Middle	$z_1 = 0$ $z_2 = b$	$z_1(t) = \big(\Omega t - (\theta_n + \theta_{st})\big)/\kappa$ $z_2(t) = (\Omega t - \theta_{st})/\kappa$
Exit	$z_1(t) = \big(\Omega t - (\theta_n + \theta_{st})\big)/\kappa$ $z_2(t) = b$	$z_1(t) = \big(\Omega t - (\theta_n + \theta_{st})\big)/\kappa$ $z_2(t) = b$

the new approach is based upon the prior work of references [10–14], the primary advantage of the current formulation is the ability to analyze delay equations in the form of state space models. Given that the the cutting forces are piecewise continuous, the temporal finite element approach will be shown to provide a natural way of discretizing the system. In particular, the cutting time was divided into temporal elements which may be conveniently truncated to capture the different limits of integration introduced in the previous section.

An expanded expression for the x-direction forces is obtained by substituting Eq. (3.3a), Eq. (3.3b), and Eq. (3.4) into Eq. (3.5). This gives the following expression,

$$F_x = \int_{z_1(t)}^{z_2(t)} -g(z,t)\Big(\frac{h + x(t) - x(t-\tau)}{2}\Big)\Big[K_t \sin 2\theta(z,t) + K_n(1 - \cos 2\theta(z,t))\Big] dz\,, \tag{3.6}$$

Equation (3.6) can be written in a more compact form as $F_x(t) = K_c(t)[x(t) - x(t-\tau)] + f_0(t)$, where $K_c(t)$ and $f_0(t)$ is compact notation for

$$K_c(t) = -1/2 \int_{z_1(t)}^{z_2(t)} [K_t \sin 2\theta(z,t) + K_n(1 - \cos 2\theta(z,t))] dz \,, \tag{3.7a}$$

$$f_0(t) = -h/2 \int_{z_1(t)}^{z_2(t)} \Big[K_t \sin 2\theta(z,t) + K_n(1 - \cos 2\theta(z,t))] dz \,. \tag{3.7b}$$

As shown in reference [48], variational system can be formed by writing the solution as perturbation $\xi(t)$ about the τ-periodic motion

$$x = x_p(t) + \xi(t) \,, \tag{3.8}$$

where $x_p(t)$ is defined as the τ-periodic motion of the tool.Substituting Eq. (3.6) and Eq. (3.8) into Eq. (3.2) and subtracting off the equation for only periodic motion gives the final equation for further study

$$\ddot{\xi} + 2\zeta\omega\dot{\xi} + \omega^2\xi = \frac{1}{m} K_c(t) \left[\xi - \xi(t-\tau)\right] \,. \tag{3.9}$$

3.4.1 State Space TFEA Approach

Time Finite Element Analysis is an approximation method that divides the time intervals of interest into a finite number of temporal elements. This approach allows the original DDE to be transformed into the form of a discrete map. The asymptotic stability of the system is then analyzed from the characteristic multipliers or eigenvalues of the map. The first step in the new approach is to write Eq. (3.9) in the form of the following state space equation,

$$\begin{bmatrix} \dot{y_1} \\ \dot{y_2} \end{bmatrix} = \begin{bmatrix} 0 & 1 \\ -\omega^2 - \frac{K_c(t)}{m} & -2\zeta\omega \end{bmatrix} \begin{bmatrix} y_1(t) \\ y_2(t) \end{bmatrix} + \begin{bmatrix} 0 & 0 \\ \frac{K_c(t)}{m} & 0 \end{bmatrix} \begin{bmatrix} y_1(t-\tau) \\ y_2(t-\tau) \end{bmatrix} , \quad (3.10)$$

where $y_1 = \xi$ and $y_2 = \dot{\xi}$. Once the governing equation is written in the state space form, it can be regarded into a more generalized form as,

$$\dot{\mathbf{y}}(t) = \mathbf{A}(t)\mathbf{y}(t) + \mathbf{B}(t)\mathbf{y}(t-\tau) , \quad (3.11)$$

where the term $\mathbf{A}(t)$ and $\mathbf{B}(t)$ are time periodic. As the delay differential equation does not have a closed form solution the TFEA method assumes an approximate solution for the equation Eq. (3.11). The assumed solution for the state and the delayed are written as linear combination of polynomials or trial function and are given as,

$$\mathbf{y}(t) = \sum_{i=1}^{3} a_{ji}^{n} \phi_i(\sigma) , \quad (3.12a)$$

$$\mathbf{y}(t-\tau) = \sum_{i=1}^{3} a_{ji}^{n-1} \phi_i(\sigma) , \quad (3.12b)$$

here a superscript is used for the coefficients to identify the n^{th} period for the current state and $n-1$ period in the delayed state variable. Each trial function, $\phi_i(\sigma)$, is written as a function of the local time, σ, within the j^{th} element and the local time is allowed to vary from zero to the time for each element, t_j. The introduction of local time variable is necessary to keep the trial functions orthogonal on the interval $0 \leq \sigma \leq t_j$. As the terms inside the matrices $\mathbf{A}(t)$ and $\mathbf{B}(t)$ are periodic, we substitute $t = \sigma + t_0$ into these matrices so that periodic terms take on the correct values over the

entire period. Here, the term t_0 is the elapsed time prior to the start of the element. The polynomials used for the analysis are,

$$\phi_1(\sigma_j) = 1 - 23\left(\frac{\sigma}{t_j}\right)^2 + 66\left(\frac{\sigma}{t_j}\right)^3 - 68\left(\frac{\sigma}{t_j}\right)^4 + 24\left(\frac{\sigma}{t_j}\right)^5 , \tag{3.13a}$$

$$\phi_2(\sigma_j) = 16\left(\frac{\sigma}{t_j}\right)^2 - 32\left(\frac{\sigma}{t_j}\right)^3 + 16\left(\frac{\sigma}{t_j}\right)^4 , \tag{3.13b}$$

$$\phi_3(\sigma_j) = 7\left(\frac{\sigma}{t_j}\right)^2 - 34\left(\frac{\sigma}{t_j}\right)^3 + 52\left(\frac{\sigma}{t_j}\right)^4 - 24\left(\frac{\sigma}{t_j}\right)^5 . \tag{3.13c}$$

These trial functions are chosen in such a way that they orthogonal and they allow the coefficients of the assumed solution the states of the system at the beginning, middle, and end of each element. Substituting Eq. (3.12a) and Eq. (3.12b) into Eq. (3.11) results in the following

$$\sum_{i=1}^{3}\Big(\mathbf{I}a_{ji}^{n}\dot{\phi}_i(\sigma) - \mathbf{A}(\sigma+t_0)a_{ji}^{n}\phi_i(\sigma) \quad - \mathbf{B}(\sigma+t_0)a_{ji}^{n-1}\phi_i(\sigma)\Big) = \text{error}\,, \tag{3.14}$$

which shows a non-zero error associated with the approximate solutions of Eq. (3.12a) and Eq. (3.12b). In order to minimize this error, the assumed solution is weighted by multiplying by a set of test functions, or so called weighting functions, and the integral of the weighted error is set to zero. This is called the method of weighted residuals, and requires that the weighting functions be linearly independent [26]. The weighting functions used for the presented analysis were shifted Legendre polynomials. These polynomials were used because they satisfy the required condition of linear independence. Here, only the first two shifted Legendre polynomials $\psi_1(\sigma) = 1$ and $\psi_2(\sigma) = 2(\sigma/t_j) - 1$ were applied. The weighted error expression becomes

$$\int_0^{t_j}\Big(a_{ji}^{n}\dot{\phi}_i(\sigma) - \mathbf{A}(\sigma+t_0)a_{ji}^{n}\phi_i(\sigma) - \mathbf{B}(\sigma+t_0)a_{ji}^{n-1}\phi_i(\sigma)\Big)\psi_p(\sigma)d\sigma = 0\,. \tag{3.15}$$

After applying each weighting function, a global matrix equation can be obtained by combining the resulting equations for each element. This equation relates the states of the system in the current period to the states of the system in the previous period. For the purposes of illustration, the two element solution would have the following global matrix

$$\begin{bmatrix} \mathbf{I} & 0 & 0 & 0 & 0 \\ \mathbf{N}_{11}^1 & \mathbf{N}_{12}^1 & \mathbf{N}_{13}^1 & 0 & 0 \\ \mathbf{N}_{21}^1 & \mathbf{N}_{22}^1 & \mathbf{N}_{23}^1 & 0 & 0 \\ 0 & 0 & \mathbf{N}_{11}^2 & \mathbf{N}_{12}^2 & \mathbf{N}_{13}^2 \\ 0 & 0 & \mathbf{N}_{21}^2 & \mathbf{N}_{22}^2 & \mathbf{N}_{23}^2 \end{bmatrix} \begin{bmatrix} a_{11} \\ a_{12} \\ a_{21} \\ a_{22} \\ a_{23} \end{bmatrix}^n = \begin{bmatrix} 0 & 0 & 0 & 0 & \mathbf{\Phi} \\ \mathbf{P}_{11}^1 & \mathbf{P}_{12}^1 & \mathbf{P}_{13}^1 & 0 & 0 \\ \mathbf{P}_{21}^1 & \mathbf{P}_{22}^1 & \mathbf{P}_{23}^1 & 0 & 0 \\ 0 & 0 & \mathbf{P}_{11}^2 & \mathbf{P}_{12}^2 & \mathbf{P}_{13}^2 \\ 0 & 0 & \mathbf{P}_{21}^2 & \mathbf{P}_{22}^2 & \mathbf{P}_{23}^2 \end{bmatrix} \begin{bmatrix} a_{11} \\ a_{12} \\ a_{21} \\ a_{22} \\ a_{23} \end{bmatrix}^{n-1}, \tag{3.16}$$

where $\mathbf{I}$ is an identity matrix and $\mathbf{\Phi}$ is the a 2×2 state transition matrix. Before proceeding, the authors note that a minimum of three elements are required to form a global matrix that truncates the temporal elements at the end of each cutting region. The terms inside the global matrix are the following square matrices

$$\mathbf{N}_{pi}^j = \int_0^{t_j} \Big(\mathbf{I}\dot{\phi}_i(\sigma) - \mathbf{A}\big(\sigma + t_0\big)\, \phi_i(\sigma) \Big) \psi_p(\sigma)\, d\sigma\,, \tag{3.17a}$$

$$\mathbf{P}_{pi}^j = \int_0^{t_j} \mathbf{B}\big(\sigma + t_0\big)\, \phi_i(\sigma) \psi_p(\sigma)\, d\sigma\,. \tag{3.17b}$$

The state transition matrix, $\mathbf{\Phi}$, provides the exact solution to the free vibration problem to account for the time intervals when the tool is not cutting. The expression for $\mathbf{\Phi}$ is

$$\Phi = \begin{bmatrix} \Phi_{11} & \Phi_{12} \\ \Phi_{21} & \Phi_{22} \end{bmatrix} . \tag{3.18a}$$

The following are the individual matrix terms

$$\Phi_{11} = \frac{\lambda_1 e^{\lambda_2 t_f} - \lambda_2 e^{\lambda_1 t_f}}{\lambda_1 - \lambda_2} , \tag{3.19}$$

$$\Phi_{12} = \frac{e^{\lambda_1 t_f} - e^{\lambda_2 t_f}}{\lambda_1 - \lambda_2} , \tag{3.20}$$

$$\Phi_{21} = \frac{\lambda_1 \lambda_2 e^{\lambda_2 t_f} - \lambda_1 \lambda_2 e^{\lambda_1 t_f}}{\lambda_1 - \lambda_2} , \tag{3.21}$$

$$\Phi_{22} = \frac{\lambda_1 e^{\lambda_1 t_f} - \lambda_2 e^{\lambda_2 t_f}}{\lambda_1 - \lambda_2} , \tag{3.22}$$

$$\tag{3.23}$$

where t_f is the time for free vibration, $\lambda_1 = -\zeta\omega + \omega\sqrt{\zeta^2 - 1}$, and $\lambda_2 = -\zeta\omega - \omega\sqrt{\zeta^2 - 1}$.

Eq. (3.16) describes a discrete time system or map that can be written in a more compact form $\mathbf{G}\mathbf{a}_n = \mathbf{H}\mathbf{a}_{n-1}$ where the elements of the $\mathbf{G}$ matrix are defined by the each $\mathbf{N}^j_{pi}$ term of Eq. (3.17a). Correspondingly, the elements of the $\mathbf{H}$ matrix are defined by the $\mathbf{P}^j_{pi}$ terms from Eq. (3.17b). Multiplying the dynamic map expression by $\mathbf{G}^{-1}$ results in $\mathbf{a}_n = \mathbf{Q}\mathbf{a}_{n-1}$ where $\mathbf{Q}= \mathbf{G}^{-1}\mathbf{H}$. Applying the conditions of the chosen trial functions to the beginning, midpoint, and end conditions allows us to replace $\mathbf{a}_n$ and $\mathbf{a}_{n-1}$ with $\mathbf{y}_n$ and $\mathbf{y}_{n-1}$, respectively. Here, $\mathbf{y}_n$ is the vector that represents the state variable at the beginning, middle, end of each temporal finite element. Thus, the the final expression becomes

$$\mathbf{y}_n = \mathbf{Q}\mathbf{y}_{n-1} , \tag{3.24}$$

The stability of the system can be directly determined from the monodromy operator **Q**, which provides a mapping over a single delay period. The eigenvalues of the monodromy operator **Q** are called characteristic multipliers (CMs). The criteria for asymptotic stability requires that the magnitudes of the CMs must be in the modulus of less than one for a given combination of the control parameters. For any CMs with magnitude greater the one, the system is considered to be unstable.

3.5 Stability Trends

The goal of this section is to apply the analysis of the previous section to investigate the influence of helix angle, radial immersion and feed direction on the stability of the experimental system. While the results of prior work have shown stability differences that can occur due to a change in the feed direction and radial immersion [58,59], the main focus here is on changes in the stability boundaries that are attributed to the tool helix angle. To be more specific, this section shows isolated islands of chatter vibration can arise for helix angle tools and that the location of the islands is different for up-milling and down-milling.

Depending on the feed direction, a milling process can be categorized as either up-milling and down-milling (see Fig. 3.3).

Fig. 3.4 shows up-milling and Fig. 3.5 shows down-milling stability charts for the system described in section two with 30^o helix angle and with changes in the radial immersion. Comparing the two figures for up-milling and down-milling, it can be observed that the period doubling lobes vary in size but are located more or less around the same spindle speed range. However this is not true for the secondary Hopf bifurcations lobes, for up-milling these Hopf bifurcations lobes are located to the left of the period doubling lobes and the for the case of down-milling they are to the right

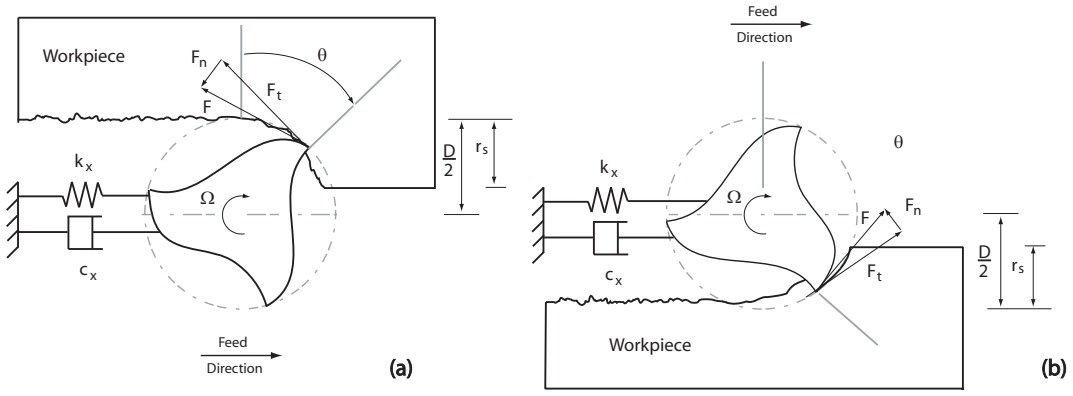

Figure 3.3: Schematic diagrams of single degree of freedom milling process: (a) Up-milling and (b) Down-milling

of the period doubling lobes , which is like a mirror image of each other. Basically the period doubling lobes are related to the impact effect of the tool entering and leaving the workpiece due which these lobes are independent of the direction of feed. Further if we look at the individual plots in each of these figures, it can be observed that as the percentage radial immersion is reduced the Hopf bifurcation lobe starts reducing in size and progressively the period doubling lobes starts to disintegrate from the Hopf bifurcation lobe. The analytical investigation becomes interesting at the point where the period doubling unstable lobe completely disintegrated from the main lobe, which is observed for 5.25% and 2% radial immersion for both up-milling Fig.(3.4c–d) and down-milling Fig.(3.5c–d) case. These disintegrated period doubling lobes are called unstable islands henceforth in the manuscript.

To confirm the existence of islands due to the effect of helix angle of the tool in the analysis, we show stability chart for different helix angles in Fig. 3.6 for the case of up-milling and Fig. 3.7 for the case of down-milling . To illustrate the effect of helix the stability plots are compared with the first subfigure in each figure, which has zero helix angle and subsequent stability charts are presented with 10^o, 30^o, and 45^o

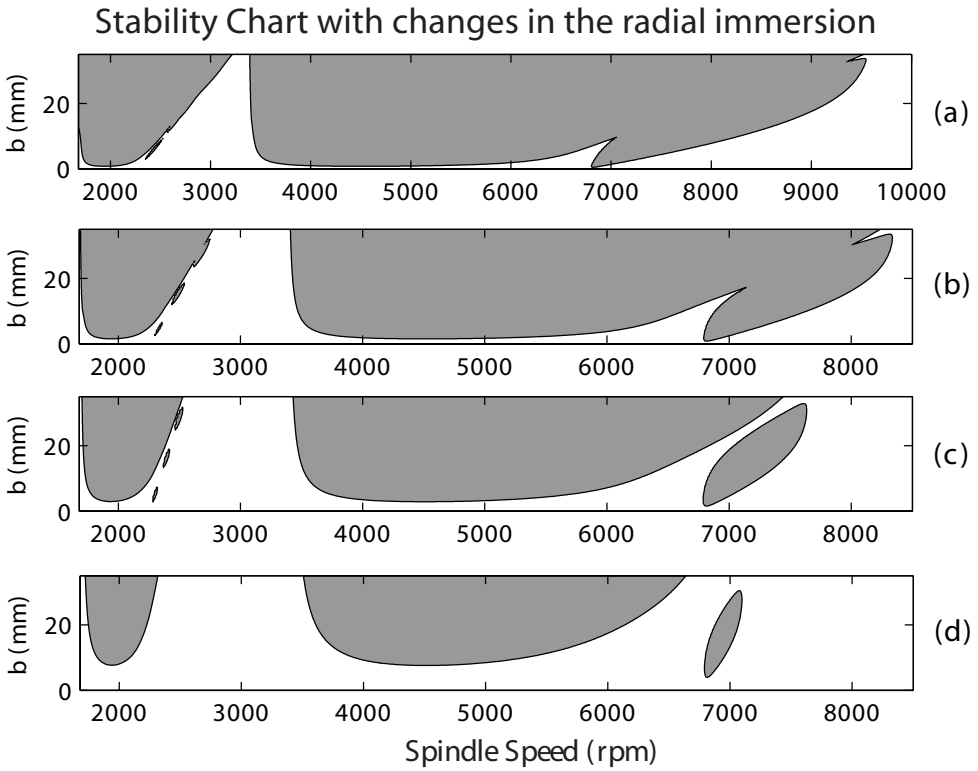

Figure 3.4: Stability Charts for Up-milling with Radial Immersion of : (a) 2% , (b) 5.25% (c) 10%, (d) 20%

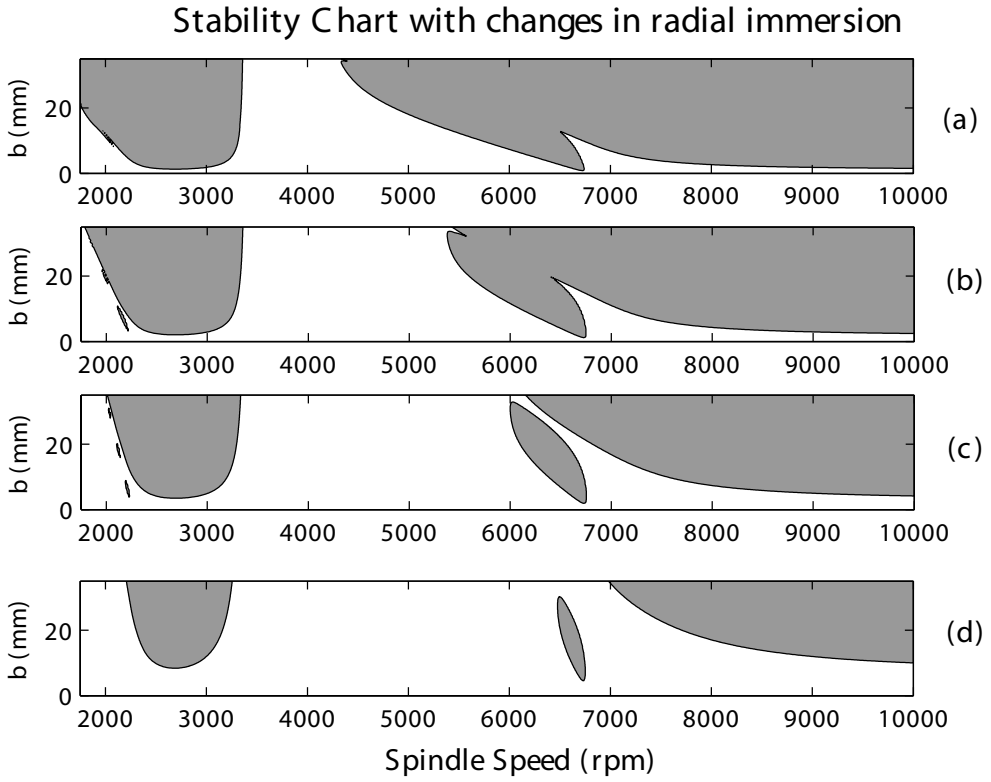

Figure 3.5: Stability Charts for Down-milling with Radial Immersion of : (a) 2% , (b) 5.25% (c) 10%, (d) 20%

helix angle. As mentioned earlier, the cutting forces change with helix angle due to which the asymptotic stability boundaries are altered. As the helix angle is increased the period doubling lobe starts to isolate from the main lobe. For the single degree of freedom system in this chapter it can be observed that for a 30^o and 45^o helix, isolated instability islands appear in the stability charts. This a new phenomenon .. (is interesting because)

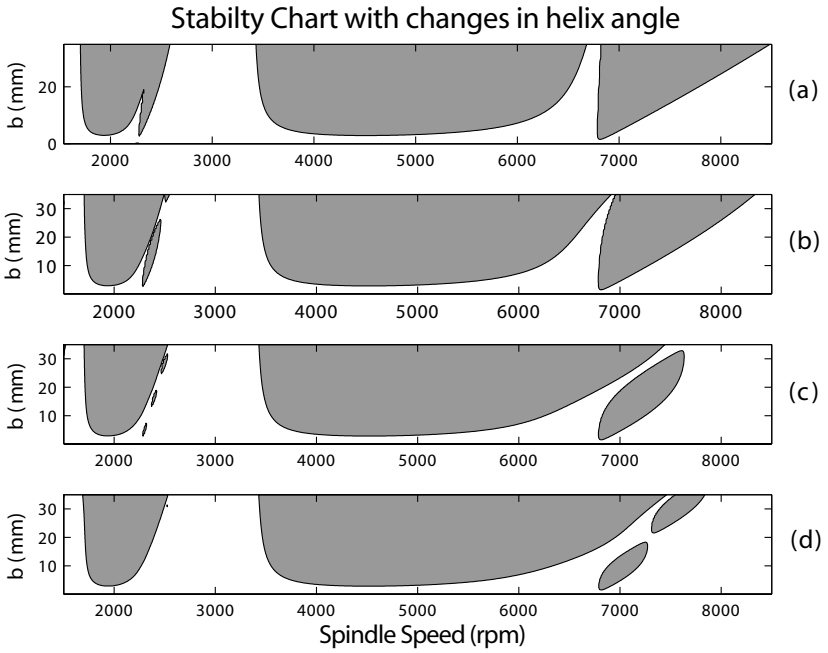

Figure 3.6: Stability Charts for Up-milling with: (a) No helix angle, (b) 10^o helix angle, (c) 30^o helix angle, (d) 45^o helix angle

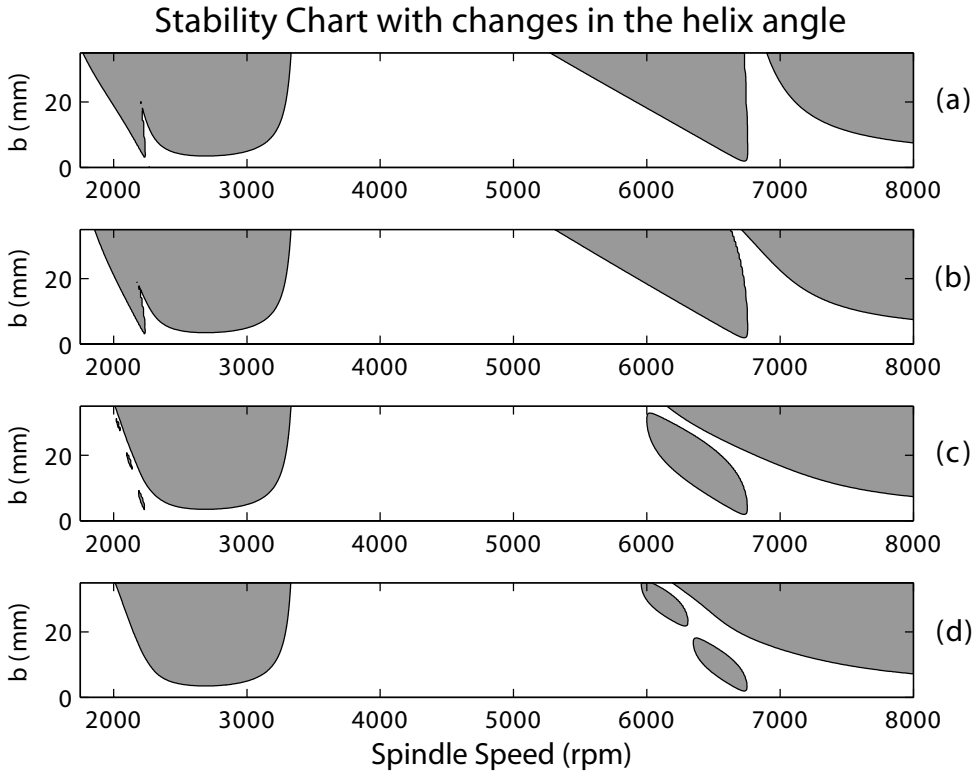

Figure 3.7: Stability Charts for Up-milling with: (a) No helix angle, (b) 10^o helix angle, (c) 30^o helix angle, (d) 45^o helix angle

3.6 Comparisons Between Theory and Experiment

This section describes the experiments that were performed to validate the phenomena of isolated islands of chatter vibration. Experiments were performed for the case of a down-milling process with 5:25% radial immersion and 30^0 helix angle. The modal parameters for the flexure system and the cutting coefficients applied for stability chart predictions are given in Table 3.1.

Figure 3.8 shows stability assessments from each cutting test superimposed onto the theoretical stability boundaries for both a 30^0 and zero helix tool. The spindle speed and cutting depths that are further described in Fig. 3.9 and Fig. 3.10, were selected to define the stability borders for the island and main Hopf bifurcation lobe.

In the figures that follow, shows time series results for eight of the cutting tests labeled $a - h$ in Fig. 3.8. For instance, the once per revolution timing pulse from the laser tachometer was used as a reference signal to periodically sample the flexure vibrations that appear in the left-hand column of Fig. 3.9 and Fig. 3.10. Since only flexure displacements were recorded, visualization of the qualitative features of each periodic attractor required the application of delayed embedding techniques to reconstruct a topologically equivalent phase space in displacement vs. delayed displacement $\theta(t + \Delta t)$ cordinates. Following the methods suggested in reference [64], algorithms were developed to graph the mutual information function for the time series and the same time series shifted by Δt. The first minimum of the mutual information graph was used as the time shift, or delay, between the original time series and the $x(t + \Delta t)$ time series. Using the false nearest neighbors approach of reference [64], the embedding dimension was found to be equivalent to two for each of the presented time series. Poincarè sections were created by periodically sampling

the displacement and delayed displacement signals as shown in the right-hand graphs of Fig. 3.9 and Fig. 3.10.

Noting the locations of tests $a - d$ in Fig. 3.8, the results of Fig. 3.9 provide experimental evidence of isolated islands of chatter vibration. As predicted by the theoretical analysis, these cases all exhibit period-doubling behavior. This type of instability is predicted when the largest magnitude eigenvalues of the monodromy operator $\mathbf{Q}$ are negative and real with a magnitude greater than one. The remaining experimental tests, experimental trials $e - h$ from Fig. 3.8, are displayed in Fig. 3.10. The first three tests are clearly stable since the both the 1/spindle period displacement samples (shown) and 1/tooth passage displacement samples (not shown) both approached a single fixed point value. Although experimental test g is a stable result, it is perhaps one of the more interesting cases since the predictions for the 30^0 and zero helix tool differ in this region of the stability chart. For instance, the zero helix angle stability predictions of Fig. 3.8 show that chatter vibrations should arise in this region for a zero helix tool, but not for a tool with a 30^0 helix.

The last experimental test shown is an example of quasi-periodic behavior and is predicted by the theoretical model when the largest complex characteristic multiplier obtains a magnitude greater than one. As shown in Fig. 3.10(h), this causes the Poincarè map for this case to take the appearance of a circle map. This final example is shown to provide evidence that the location of the secondary Hopf bifurcation region is also correctly captured.

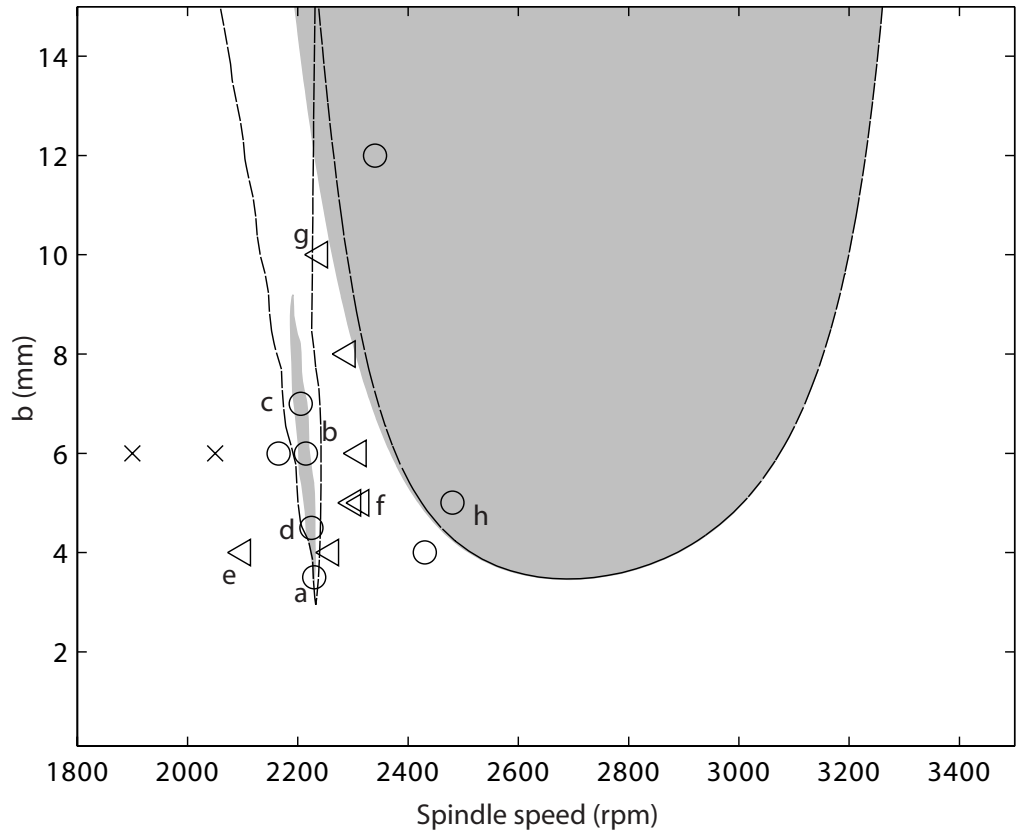

Figure 3.8: Shaded stability chart with 30^o helix angle is superimposed zero helix case. Symbols in the above diagram are as follows: (1)($\triangleleft$) is clearly stable case, (2)($\circ$) is an unstable cutting case, and (3)($\times$) are points that are not clearly stable or unstable

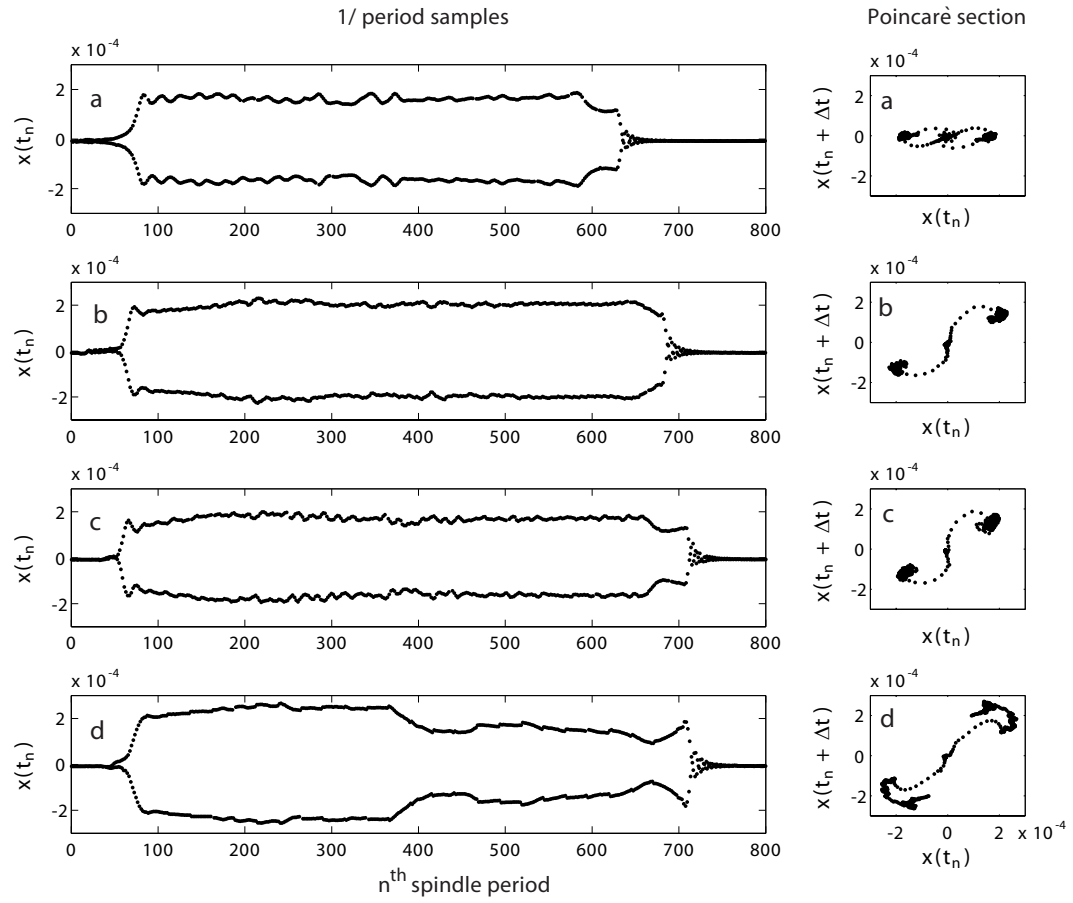

Figure 3.9: Experimental down-milling data for cases: (a) Ω=2230 (rpm) and b=3.5 (mm), (b) Ω=2215 (rpm) and b=6 (mm) (c) Ω=2205 (rpm) and b=7 (mm) (d) Ω=2225 (rpm) and b=4.5 (mm) shown in the Fig. 3.8. Each row contains 1/period samples plot in the compliant x-direction and poincaré section shown in displacement and delayed displacement co-ordinates. All the case are clearly unstable showing period doubling.

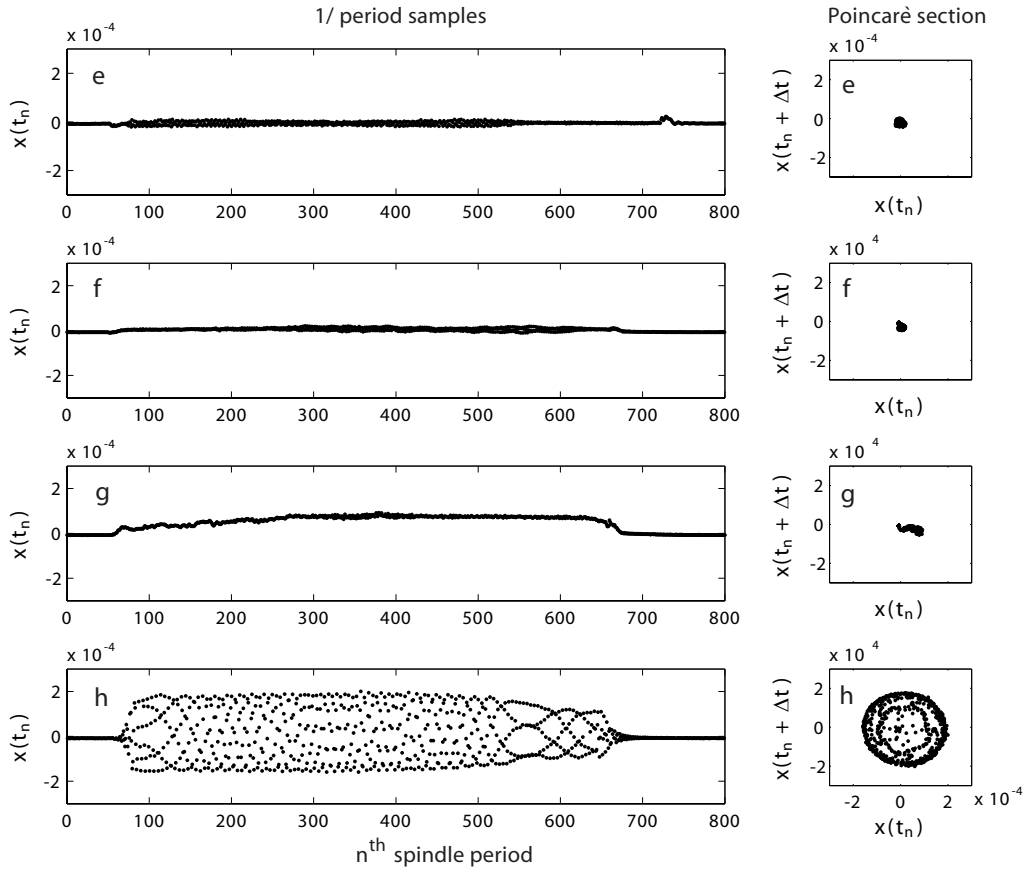

Figure 3.10: Experimental down-milling data for cases: (e) Ω=2100 (rpm) and b=4 (mm), (f) Ω=2300 (rpm) and b=5 (mm), (g) Ω=2240 (rpm) and b=10 (mm), (h) Ω=2480 (rpm) and b=5 (mm) shown in the Fig. 3.8. Each row contains 1/period samples plot in the compliant x-direction and poincaré section shown in displacement and delayed displacement co-ordinates. Cases (e),(f) and (g) show stable solution and (h) shows an unstable solution.

3.7 Conclusions

This chapter explores the in fluence of a common form of tool geometry on the stability trends of a milling process. Modeling efforts consider the in uence of the tool helix angle to obtain an analytical force model with three piecewise continuous regions of cutting. A new theoretical analysis is described that is applicable to solving the governing equations that arise. The new analysis is then applied to examine the asymptotic stability trends for several different radial immersions and helix angles.

The most interesting phenomena is the presence of isolated islands of chatter vibration. However, we have also shown stability differences between the islands and secondary Hopf bifurcation lobes for up-milling and down-milling. Additional studies, for this particular system, show that the zero helix angle tool does not result in isolated islands of chatter. Finally, theoretical predictions are validated by a series of experimental down-milling experiments which confirm the isolated island phenomenon.

Chapter 4

Summary

A new approach of state space formulation method of temporal finite element analysis (TFEA) is developed to investigate the stability behaviour of linear autonomous and non-autonomous delay differential equations (DDE's), which is applicable to a broader class of problems. The previous work in TFEA was limited to second order DDE's and as this new approach is based on state space appraoch, the stability behaviour of systems that can be written in state space model can be investigated. To validate the applicability of the method several problems which appeared in prior work are analyzed in the second chapter. The main focus here was to be able to develop method which is simpler and can be applied to stability analysis of an milling process. Stability plots are obtained for single degree of freedom milling equation and compared with prior work by Mann and Young [13] using the same cutting forces and modal parameters and these plots were in perfect agreement. The state space approach presented in the thesis can deal with delay differential equation with single delay only, however further extension of this method for stability analysis of multiple delay DDE's could be potentially important area of further research.

The invesitgation of stability behaviour considering the influence of helix angle of

the tool for a single degree of freedom milling equation showed interesting phenomena of isolated islands of chatter vibration in the stability charts. Further comparison for different helix angle cases showed distinctive trends in the stability chart. These islands were obsereved in the analytical stability charts for certain radial immersion. This served as a motivation to perform experiments and validate the existence of the isolated islands. Detailed experiment was performed on the basis of which conclusive remarks can be made on the presence of isolated islands in milling. Islands of instability in milling with experimental results was given by Zatarain *et. al* [9] . However this validation could not rule out the effect of runout which is a common phenomenon affecting the cutting performance. Espeacially in case of period doubling it is difficult to distinguish between run-out and period doubling if end mill with even numbered teeth is used for the experiments, however with odd number of teeth on the end mill, each tooth passage signal can be analyzed in order to distinguish between period doubling and run-out. And for these reason the experimental analysis in this thesis could provide conclusive evidence of isloated islands of instability.

The experimental evidence of isolated islands is limited to the case of down-milling. With distinct difference in the stability boundaries for up-milling and down-milling, it is of potential importance to also validate the results for up-milling where these islands appear in the stability chart.

Bibliography

[1] R. N. Arnold, "Mechanism of tool vibration in cutting of steel," *Proceedings of the Institution of Mechanical Engineers*, vol. 154, pp. 261–276, 1946.

[2] J. Tlusty and M. Polacek, "The stability of machine tools against self-excited vibrations in machining," *ASME International Research in Production Engineering*, pp. 465–474, 1963.

[3] S. A. Tobias, *Machine Tool Vibration*. London: Blackie, 1965.

[4] S. A. Tobias and W. Fishwick, *A Theory of Regenerative Chatter*. 1958.

[5] J. Tlusty and F. Ismail, "Basic nonlinearity in machining chatter," *Annals of the CIRP*, vol. 30, pp. 21–25, 1981.

[6] J. Tlusty, *Manufacturing Processes and Equipment*. Upper Saddle River, NJ: Prentice Hall, 1 ed., 2000.

[7] S. Smith and J. Tlusty, "An overview of the modeling and simulation of the milling process," *Journal of Engineering for Industry*, vol. 113, pp. 169–175, 1991.

[8] D. Montgomery and Y. Altintas, "Mechanism of cutting force and surface generation in dynamic milling," *Journal of Engineering for Industry*, vol. 113, pp. 160–168, 1991.

[9] M. Zatarain, J. M. noa, G. Peigné, and T. Insperger, "Analysis of the influence of mill helix angle on chatter stability," *Annals of the CIRP*, 2006. in press.

[10] J. E. Halley, "Stability of low radial immersion milling," 1999. Master's thesis, Washington University, Saint Louis.

[11] P. V. Bayly, J. E. Halley, M. A. Davis, and J. R. Pratt, "Stability analysis of interrupted cutting with finite time in the cut," 2001.

[12] B. P. Mann, P. V. Bayly, M. A. Davies, and J. E. Halley, "Limit cycles, bifurcations, and accuracy of the milling process," *Journal of Sound and Vibration*, vol. 277, pp. 31–48, 2004.

[13] B. P. Mann and K. A. Young, "An empirical approach for delayed oscillator stability and parametric identification," *Proceedings of the Royal Society A*, vol. 462, pp. 2145–2160, 2006.

[14] B. P. Mann, K. A. Young, T. L. Schmitz, and D. N. Dilley, "Simultaneous stability and surface location error predictions in milling," *Journal of Manufacturing Science and Engineering*, vol. 127, pp. 446–453, 2005.

[15] B. Balachandran, "Non-linear dynamics of milling process," *Proceedings of the Royal Society of London A*, vol. 359, pp. 793–819, 2001.

[16] T. Insperger and G. Stépán, "Remote control of periodic robot motion," in *Proceedings of 13th CISM-IFToMM Symposium on Theory and Practice of Robots and Manipulators*, pp. 197–203, 2000.

[17] J. J. Batzel and H. T. Tran, "Stability of the human respiratory control system. part i: Analysis of a two-dimensional delay state-space model," *Journal of Mathematical Biology*, vol. 41, pp. 45–79, 2000.

[18] G. Stépán, "Modelling nonlinear regenerative effects in metal cutting," *Philosophical Transactions of the Royal Society of London A*, vol. 359, pp. 739–757, 2001.

[19] N. Olgac and R. Sipahi, "A unique methodology for chatter stability mapping in simultaneous machining," *Journal of Manufacturing Science and Engineering*, vol. 127, pp. 791–800, 2005.

[20] P. V. Bayly, J. E. Halley, B. P. Mann, and M. A. Davis, "Stability of interrupted cutting by temporal finite element analysis," *Journal of Manufacturing Science and Engineering*, vol. 125, pp. 220–225, May 2003.

[21] G. Stépán, *Retarded Dynamical Sytems: Stability and Characteristic Functions*. John Wiley & Sons, 1989.

[22] J. K. Hale and S. V. Lunel, *Introduction to functional differential equations*. New York: Springer-Verlag, 1993.

[23] T. Insperger and G. Stépán, "Stability chart of the delayed mathieu equation.," *Proceedings of Royal Society of London A*, vol. 458, pp. 1989–1998, 2002.

[24] B. P. Mann, P. V. Bayly, M. A. Davies, and J. E. Halley, "Limit cycles, bifurcations, and accuracy of the milling process," *Journal of Sound and Vibration*, vol. 277, pp. 31–48, 2004.

[25] T. Insperger and G. Stépán, "Semi-discretization method for delayed systems," *International Journal for Numerical Methods in Engineering*, vol. 55(5), pp. 503–518, 2002.

[26] J. N. Reddy, *An Introduction To The Finite Element Method*. New York, NY: McGraw-Hill, Inc., 2 ed., 1993.

[27] T. Kálmar-Nagy, "A new look at the stability analysis of delay differential equations," in *Proceedings of International Design Engineering Technical Conferences*

and Computers and Information in Engineering Conference, Long Beach, California, DETC2005-84740, ASME, 2005.

[28] N. K. Garg, B. P. Mann, N. H. Kim, and M. H. Kurdi, "Stability of a time-delayed system with parametric excitation," *Journal of Measurement and Control*. – Accepted and in Press since 2005.

[29] G. Stépán, "Vibrations of machines subjected to digital force control," *International Journal of Solids and Structures*, vol. 38, pp. 2149–2159, 2001.

[30] C. S. Hsu and S. J. Bhatt, "Stability charts for second order dynamical systems with time lag," *Journal of Applied Mechanics (ASME)*, vol. 33E(1), pp. 119–124, 1966.

[31] B. Mann and K. Young, "An empirical approach to stability and parametric identification in time delayed dynamical systems," *Proceedings of the Royal Society of London A*, vol. 462, pp. 2145–2160, 2006.

[32] T. Schmitz and B. Mann, "Closed form solutions for the prediction of surface location error in milling," *International Journal of Machine Tools and Manufacture*, vol. 46, pp. 1369–1377, 2006.

[33] P. V. Bayly, J. E. Halley, B. P. Mann, and M. A. Davis, "Stability of interrupted cutting by temporal finite element analysis," *Journal of Manufacturing Science and Engineering*, vol. 125, pp. 220–225, May 2003.

[34] E. Mathieu, "Memoire sur le mouvement vibratorie d'une membrane de forme elliptique," *J. Math*, vol. 13, pp. 137–203, 1868.

[35] K. Bellman, R.and Cooke, *Differential-difference equations*. Academic, 1963.

[36] S. J. Bhatt and C. S. Hsu, "Stability criteria for second-order dynamical systems with time lag," *Applied Mechanics*, vol. 33, pp. 113–118, 1966.

[37] L. Pontryagin, "On the zeros of some elementary transcendental functions," *Izv. Akad. Nauk SSSR*, vol. 6, pp. 115–134, 1942.

[38] T. Insperger and G. Stépán, "Updated semi-discretization method for periodic delay-differential equations with discrete delay.," *International Journal for Numerical Methods*, vol. 61, pp. 117–141, 2004.

[39] T. Insperger and G. Stépán, "Semi-discretization of delayed dynamical systems," in *Proceedings of Design Engineering Technical Conferences and Computers and Information in Engineering Conference, Pittsburgh, Pennsylvania*, DETC2001/VIB-21446, ASME, 2001.

[40] B. P. Mann, N. K. Garg, K. A. Young, and A. M. Helvey, "Milling bifurcations from structural asymmetry and nonlinear regeneration," *Nonlinear Dynamics*, vol. 42, pp. 319–337, 2005. No. 4.

[41] Y. Altintas and E. Budak, "Analytical prediction of stability lobes in milling," *CIRP Annals*, vol. 44, no. 1, pp. 357–362, 1995.

[42] Y. Altintas, *Manufacturing Automation*. New York, NY: Cambridge University Press, 1 ed., 2000.

[43] T. Schmitz and J. Ziegert, "Examination of surface location error due to phasing of cutter vibrations," *Precision Engineering*, vol. 23, pp. 51–62, 1999.

[44] B. P. Mann, T. Insperger, P. V. Bayly, and G. Stépán, "Stability of up-milling and down-milling, part 2: Experimental verification," *International Journal of Machine Tools and Manufacture*, vol. 43, pp. 35–40, 2003.

[45] T. Insperger, B. P. Mann, G. S. án, and P. V. Bayly, "Stability of up-milling and down-milling, part 1: Alternative analytical methods," *International Journal of Machine Tools and Manufacture*, vol. 43, pp. 25–34, 2003.

[46] T. Insperger and G. Stépán, "Comarison of the stability lobes for up- and down-milling," *Proceedings of Dynamics and Control of Mechanica Processing Workshop*, no. 2nd Workshop, pp. 53–57, 2001. Budapest University of Technology and Economics, Budapest.

[47] N. D. Sims, "The self-excitation damping ratio: A chatter criterion for time domain simulations,"

[48] B. P. Mann and P. V. Bayly, "An empirical approach for delayed oscillator stability and parametric identification," *Proceedings of the Royal Society A*, vol. 462, pp. 2145–2160, 2006.

[49] M. A. Davies, J. R. Pratt, B. Dutterer, and T. J. Burns, "Stability prediction for low radial immersion milling," *Journal of Manufacturing Science and Engineering*, vol. 124, no. 2, pp. 217–225, 2002.

[50] I. Minis and R. Yanushevsky, "A new theoretical approach for prediction of machine tool chatter in milling,"

[51] J. Tlusty and F. Ismail, "Special aspects of chatter in milling,"

[52] M. Davies and B. Balachandran, "Impact dynamics in milling of thin-walled structures,"

[53] N. H. Hanna and S. A. Tobias, "A theory of nonlinear regenerative chatter,"

[54] M. Wiercigroch and E. Budak, "Sources of nonlinearities chatter generation and suppression in metal cutting,"

[55] M. Davies and T. Burns, "Thermomechanical oscillations in material flow during high-speed machining,"

[56] I. Grabec, "Chaotic dynamics of the cutting process,"

[57] W. T. Corpus and W. J. Endres, "A high order solution for the added stability lobes in intermittent machining," *Proceeding of the Symposium on Machining Processes*, no. MED-11, pp. 871–878, 2000.

[58] T. Insperger, B. P. Mann, G. Stépán, and P. V. Bayly, "Stability of up-milling and down-milling, part 1: Alternative analytical methods," *International Journal of Machine Tools and Manufacture*, vol. 43, pp. 25–34, 2003.

[59] B. P. Mann, T. Insperger, P. V. Bayly, and G. Stépán, "Stability of up-milling and down-milling, part 2: Experimental verification," *International Journal of Machine Tools and Manufacture*, vol. 43, pp. 35–40, 2003.

[60] R. Szalai and G. Stépán, "Lobes and lenses in interrupted turning," *Journal of Computational and Nonlinear Dynamics*. in, press.

[61] S. Smith, *Elements of Elastic Mechanisms*. London: Taylor and Francis, Inc, 2000.

[62] M. E. Martellotti, "An analysis of the milling process," *Transactions of the ASME*, vol. 63, pp. 677–700, 1941.

[63] M. E. Martellotti, "An analysis of the milling process. part ii: Down milling," *Transactions of the ASME*, vol. 67, pp. 233–251, 1945.

[64] H. D. Abarbanel, *Analysis of Observed Chaotic Data*. Institute for Nonlinear Science, New York, NY: Springer, 1996.